Ultrasonographic circumferential strain pattern analysis of the cardiac septal wall in rodents with experimental pulmonary hypertension.

BY

CHARL FRANCOIS CORNELIS VAN HEYNINGEN

STUDENT NUMBER – VHYCHA001

SUBMITTED TO THE UNIVERSITY OF CAPE TOWN

In fulfilment of the requirements for the degree:

Master of Medicine (MMED) in Anaesthesiology

Faculty of Health Sciences

University of Cape Town

DATE OF SUBMISSION: 13 April 2023

Institution: Department of Anaesthesiology and Peri-Operative Medicine

Groote Schuur Hospital

Anzio road, Observatory, Cape Town

Phone: 021 404 5001

Supervisor:

Dr. Nkanyiso Hadebe

Co-supervisors:

Prof. Justiaan Swanevelder

Dr. Marcelle Jagga

DECLARATION

I, ………………………………, hereby declare that the work on which this dissertation/thesis is based is my original work (except where acknowledgements indicate otherwise) and that neither the whole work nor any part of it has been, is being, or is to be submitted for another degree in this or any other university.

I empower the university to reproduce for the purpose of research either the whole or any portion of the contents in any manner whatsoever.

Signature: …………………………………

Date: …………………………………

TABLE OF CONTENTS

LIST OF ABBREVIATIONS

cMRI	- cardiac magnetic resonance imaging
CO	- cardiac output
CS	- circumferential strain
EF	- ejection fraction
hPAH	- heritable pulmonary arterial hypertension
IV	- interventricular
IQR	- interquartile range
LS	- longitudinal strain
LV	- left ventricle
LVEDV	- left ventricular end diastolic volume
MCT	- monocrotaline
mPAP	- mean pulmonary artery pressure
PAAT	- pulmonary artery acceleration time
PAH	- pulmonary arterial hypertension
PASP	- pulmonary artery systolic pressure
PAWP	- pulmonary artery wedge pressure
PH	- pulmonary hypertension
PVR	- pulmonary vascular resistance
RAP	- right atrial pressure
RH	- right heart
RHC	- right heart catheterisation
RS	- radial strain

RV	- right ventricle
RVDP	- right ventricular diastolic pressure
RVEDV	- right ventricular end diastolic volume
RVF	- right ventricular failure
RVHF	- right ventricular heart failure
SPAP	- systolic pulmonary artery pressure
STE	- speckle tracking echocardiography
WHO	- World Health Organisation

SECTION ONE – LITERATURE REVIEW

INTRODUCTION

The function of the right heart (RH) is complex, and traditionally difficult to assess in the clinical setting. At the same time, changing functional parameters of the right heart are recognised as predictors of mortality in a variety of diseases, and are therefore useful in the clinical setting to guide diagnosis and management of these conditions.(1)

Echocardiography is a cost-effective and noninvasive investigation of cardiac function, with ongoing technological advances significantly improving the usefulness of this imaging modality. Echocardiography has been extensively used in the diagnosis and evaluation of pulmonary arterial hypertension (PAH), but limitations remain with this imaging technique, especially early in the clinical course of the disease.

Since the development of ultrasonography, many echocardiographic parameters of right heart function have been investigated. From these, complex derivations as well as scoring systems have also been described in an attempt to quantify a decline in-, or abnormalities of right heart function.

Myocardial deformation analysis using speckle tracking echocardiography (STE) has been developed over the past decade as a novel method of assessing myocardial function.(2)

The aim of our study was to assess the changes in circumferential strain (CS) of the septal wall of rats with monocrotaline(MCT)-induced pulmonary arterial hypertension (PAH).

PULMONARY ARTERIAL HYPERTENSION

PAH is defined as mean pulmonary arterial pressures of >20 mmHg at rest, and is characterised by increased pulmonary arterial resistance due to vascular remodelling.(3)

Prevalence of the disease is estimated to be between 10 and 52 cases per million,(4) although reliable statistics are lacking for sub-Saharan Africa.

Progression of pulmonary arterial hypertension results in anatomical, mechanical and functional changes in the right heart. Left untreated, 5-year survival is only 57%.(5)

Early diagnosis and treatment is associated with improved outcomes in PAH. Non-specific symptoms and subtleties in clinical findings can delay diagnosis of the condition.(6)

Pulmonary Arterial Hypertension in rodents and Ultrasonography

Experimental pulmonary hypertension in a rodent model is widely used to investigate the pathophysiological process of PAH and right ventricular heart failure. The model has proven essential in exploration of new diagnostic and therapeutic techniques. Chemically induced PAH in rodents results in typical features of right ventricular (RV) failure, which are predictable and reproducible.(7)

Echocardiography is used extensively in the diagnosis and workup of right heart pathology, as well as prognostication. Availability of trained operators and appropriate equipment has improved across many healthcare settings. Nevertheless, imaging of the right heart remains a challenge, and can often only be performed by dedicated echocardiology units or highly skilled operators. In addition, echocardiography alone is inaccurate in estimating pulmonary artery systolic pressures (PASP).(8)

Advances in technology have allowed novel echocardiographic parameters to be developed. More recently, speckle tracking echocardiography has allowed strain pattern analysis of the heart and its structures, providing new insights into cardiac pathology.(9)

Strain pattern analysis relies on software which tracks the movement of ‘speckles’ within the ultrasound image, allowing quantification of the deformation of the imaged tissue, such as cardiac muscle. This data is presented in various forms, including graphically, allowing for rapid identification of abnormal patterns, which may indicate a pathological process.

Although rodent hearts have been imaged extensively, limited data exists on speckle tracking echocardiography and strain pattern analysis of the right heart. No data exists regarding segmental analysis of the septal wall alone in RH pathology.(10)

Limitations and difficulties of transthoracic echocardiography persist, and skilled operators are required to obtain unobscured views of the right heart.

Transthoracic views of the left side of the heart, including the septal wall, are far easier to obtain. The left heart is not as obscured by the sternum, and sonic windows between ribs allow for relatively easy access to the heart.

The functional relationship between the left and right heart is complex. The term ventricular interdependence (or ventricular coupling) describes the phenomenon that alteration in the pressure or filling of one ventricle affects the functional characteristics of the other. This phenomenon also leads to abnormal septal motion, which is well described by other forms of cardiac imaging.(11)

In rodents, pulmonary arterial acceleration time is a validated ultrasonographic measure correlating with the onset and progression of raised pulmonary pressures.(2)

In a recent echocardiography study analysing the entire right heart in rodents with experimental pulmonary hypertension, circumferential strain analysis showed promise. CS analysis showed good correlation with other, validated echocardiographic features of pulmonary hypertension and right ventricular heart failure. However, the authors noted that reproducibility and diagnostic utility were limited, suggesting that further research be conducted.(10)

Many of the challenges associated with ultrasonographic assessment of the entire right heart are irrelevant if one focuses on the interventricular septal wall as a segment. This structure can be imaged consistently through transthoracic echocardiographic windows. Strain pattern analysis can be reliably applied, without the need to image the entire right heart.

Research Question

In experimental pulmonary hypertension, does the echocardiographic strain pattern of the interventricular septal wall correlate with the development and degree of pulmonary hypertension?

SIGNIFICANCE

Circumferential strain decrease, if shown to correlate with the presence and severity of PAH in rodents, will be significant in allowing relatively inexperienced operators to diagnose and stage the disease without the need for extensive ultrasonographic imaging.

LITERATURE REVIEW

Despite significant advances in many aspects of medicine, pulmonary arterial hypertension persists as a devastating disease. The aetiologies are varied, but all result in progressive increase in pulmonary vascular resistance through the mechanism of progressive occlusive vasculopathy. The disease affects individuals of all ages, gender and race, although it is considered a rare entity.(12, 13)

Pulmonary hypertension encompasses a group of diseases characterised by a resting mean pulmonary arterial pressure of greater than 25 mmHg. PAH is categorised into 1 of 5 groups by the World Health Organisation (WHO), and is further subdivided by aetiology.(3, 14)

The disease is characterised by endothelial dysfunction and inflammation, as well as smooth muscle proliferation, leading to increased resistance in the pulmonary vasculature. The resultant raised pulmonary pressures leads to right heart failure, and eventual death if left untreated.(14)

PHYSIOLOGY

The pulmonary trunk arises from the right ventricular outflow tract, divides into the left and right pulmonary circulations, which rapidly branch into a large network of functional capillaries. These lie adjacent to alveoli (the alveolar capillaries) and allow for efficient gaseous exchange, while others lead to and from the alveoli and are not involved in gaseous exchange (the extra-alveolar capillaries). Corresponding venules drain oxygenated blood into the pulmonary venous system and subsequently into the left side of the heart and systemic circulation.(1, 15)

The pulmonary and systemic circulations lie in series, and therefore total blood flow is (almost) equal for both systems. It is theorised that the dual circulation is the result of an evolutionary process aimed at protecting the delicate gaseous exchange membrane from the high pressures required for organ perfusion. Some significant differences exist between these systems.(15)

In healthy individuals, the pulmonary circulation is a high-flow, low pressure system. In contrast to the systemic arterial system, pulmonary vessels are thin-walled, distensible and compliant, offering minimal resistance to flow and with significant redundancy regarding increases in volume. Therefore, increases in cardiac output (CO) are easily accommodated by the pulmonary vasculature and do not result in raised mPAP in healthy individuals. In higher output states such as during exercise, there is significant recruitment and distension of arterioles which further accommodates the raised CO. At most, modest increases in pressure are seen under these physiological conditions.(1, 16, 17)

This has also led to ongoing discussion regarding the value of measuring pulmonary pressures during exercise as a means of unmasking early onset PAH.

A variation of Ohm's Law, as well as Poiseuille's Law, provides the basis for understanding the physiological determination of mean pulmonary arterial pressure (mPAP), where:

- mPAP = (right ventricle cardiac output x pulmonary vascular resistance) + alveolar occlusion pressure.(1)

and

- PVR = (length . viscosity . 8) / (π . r^4)

  = (mPAP – mean left atrial pressure) / (pulmonary blood flow)

  = $\Delta P/Q$

These equations are extrapolated to human physiology from physical laws describing the laminar, non-pulsatile flow of fluid through non-distensible cylindrical tubes under laboratory conditions. Despite limitations due to this incongruity, the equations serve to describe pulmonary physiology to a large degree.(15)

The limits of pulmonary vascular pressures are dependent on sex and age. Women have a lower cardiac output due to smaller size, and therefore a greater pulmonary vascular resistance (PVR). These differences disappear once adjusted for age. PAP also increases with increasing age.(16)

In normal physiology, PVR is determined by, and changes in response to, a variety of factors. These include body position in relation to gravity, degree of lung distension, transmural lung pressure, as well as biologically active molecules and neurohormonal factors.(1, 15)

Increased by	Decreased by
Increased $PaCO_2$	Decreased $PaCO_2$
Decreased pH	Increased pH
Decreased PaO_2	Increased PaO_2
Adrenaline (epinephrine)	Isoprenaline
Noradrenaline (norepinephrine)	Acetylcholine
Thromboxane A_2	Prostacyclin (prostaglandin I_2)
Angiotensin II	Nitric oxide (NO)
Serotonin (5-hydroxytryptamine)	Increased peak airway pressure
Histamine	Increased pulmonary venous pressure
High or low lung volume	Volatile anaesthetic agents

Table 1. A non-exhaustive list of some factors influencing pulmonary vascular resistance. Taken from *Physics, Pharmacology and Physiology for Anaesthetists; ME Cross, EVE Plunkett; Cambridge University Press; P 201-238.(2014).* $PaC0_2$ – partial pressure of carbon dioxide; PaO_2 – partial pressure of oxygen.

In addition, there are dynamic mechanical factors which affect PVR at a capillary level. During inspiration, enlarging alveoli cause stretching and elongation of alveolar capillaries which raise the PVR. At the same time, extra-alveolar capillaries are stretched radially with negative transpleural pressures, resulting in a decrease in PVR. The converse occurs during expiration.(15)

Blood viscosity, as well as the pulsatile nature of the flow, add further complexity to our understanding of pulmonary haemodynamics.

If all of these factors are considered, it becomes clear that human physiology is more complex than the laws of physics which are used to describe it.

THE RIGHT HEART

The right heart is functionally coupled to the pulmonary circulation, and acts as a conduit suited to high flow and low pressure circulation.

It is situated immediately posterior to the sternum, and anatomically divided into an inflow tract (sinus), the trabeculated apical myocardium, as well as an outflow tract (conus). In cross-section, the right ventricle has a complex crescent-shaped geometry, with muscle fibre bundles arranged in interlacing spirals, and is triangular in side-view.(18-20)

The RV myocardium is thin relative to the LV, and itself has 2 distinct muscle layers. Those of the external layer are arranged circumferentially, and the inner layer are arranged longitudinally. Common, encircling epicardial fibres and a shared septal wall create a functional interdependence between the left and right ventricles known as ventricular coupling or ventricular interdependence.(18, 19)

Contraction occurs in a peristaltic fashion from the inflow to outflow tract. The main component of RV function is due to longitudinal shortening, while ventricular coupling may account for up to 40% of the RV function through traction of the RV free wall toward the conical septum, creating a bellows effect. Circumferential shortening is the third mechanism of RV function.(19)

As in the LV, the RV function reflects preload, contractility and afterload. However, heart rhythm, ventricular synchronicity, valvular pathology, as well as the force-interval relationship of the RV also influence function.(20)

For the purposes of this paper, the effects of afterload on RV function must be considered. As mentioned, the right heart-pulmonary circulation system is one of high volume but low pressure. As such, the RV is highly sensitive to changes in pressure as manifested by a rapidly decreased output, where stroke volume is inversely related to afterload (Figure 1).

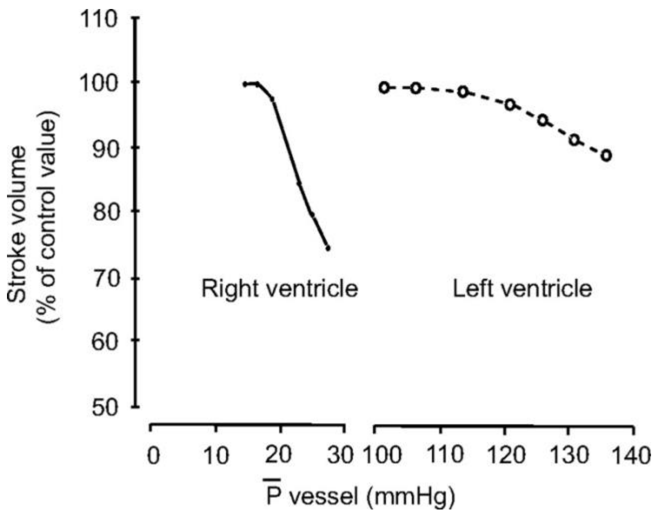

Figure 1: Comparative stroke volume responses of the RV and LV to increases in afterload. P – pressure in mmHg.(21)

Ventricular Interdependence

Ventricular interdependence can broadly be defined as "the forces that are transmitted from one ventricle to the other through the myocardium and the pericardium, independent of neural, humoral, or circulatory effects".(22)

More specifically, this is the concept that the shape, size and compliance of each ventricle affects the pressure-volume relationship, shape and size of the other. Experimental animal studies show that up to 40% of RV function is reliant on this mechanism.(20, 22)

Further, interdependence can be divided into diastolic and systolic components. Diastolic interdependence refers to the lusitropy, or diastolic compliance, of one ventricle as being partly dependent on the volume of the other. The pericardium plays an important role in this physiological process. Systolic interdependence refers to the mutual contribution of contraction of one ventricle to the function of the other. In healthy individuals it is predominantly the RV which benefits from LV contraction.(19)

The role of the interventricular septum in ventricular interdependence is complex and incompletely understood, but it is known to mediate systolic interdependence. Because of the position between the ventricles, it is key in their interaction.(18, 20)

Volume and Pressure Overload States

The so-called reverse Bernheim effect, where RV pressure and volume overload due to atrial-septal defects caused impaired LV function, has been described as early as 1957 by Dexter. A leftward shift of the IV septum was noted which, he postulated, caused impaired LV filling.(23)

It has since been well established that these changes do occur, along with significant cardiodynamic changes in the septum and LV.(22, 23)

In right sided volume overloaded states with relatively normal pressures, ejection fraction (EF) is preserved and RV end- diastolic volume (RVEDV) is increased. The septum is shifted to the left, resulting in impaired LV function due to decreased LV end diastolic volume (LVEDV) and EF.

In pressure overloaded states, there is also increased RVEDV and decreased EF, with a decrease in septal stiffness but an increase in RV free wall stiffness.

These abnormal states result in inhomogeneous and asynchronous contraction of the RV, particularly since increased afterload creates prolonged contraction.(24)

There is a progressively impaired interaction between the ventricles, resulting in ventricular dis-synchrony and septal wall motion abnormalities as seen on cardiac magnetic resonance imaging (cMRI), as well as other modalities.(25)

Septal position shifts progressively to the left heart, initially flattening and thereafter bowing into the left ventricle as volume and pressure in the RV increase. Secondly, dynamic septal movement becomes abnormal during the cardiac cycle.

Blood Supply

Blood supply varies, with approximately 80% of the population having right-dominant supply where most of the RV is supplied by the right coronary artery. The posterior wall is supplied by the posterior descending artery, and the anteroseptal region by the left anterior descending artery. Functionally, perfusion of the RV with normal pressures occurs during both systole and diastole, while more marginal areas, such as the lateral wall, enjoy perfusion only during diastole.(19, 20)

In addition, the RV is considered relatively resistant to ischaemia; this is likely due to 3 factors; lower oxygen consumption (due to lower wall tensions), increased oxygen extraction, and a more extensive collateral blood supply.(20)

Pulmonary Hypertension

Pulmonary hypertension (PH) is a disease of significant concern. Global prevalence is estimated to be 1%, rising to 10% of the population of individuals over 65 years of age. It affects all age groups and genders, and carries with it a significant mortality risk.(26)

Definition

PH is a clinical condition defined by a mean resting pulmonary arterial pressure (mPAP) of greater than 20 mmHg, measured using right heart catheterisation (RHC), whilst supine. PH was previously arbitrarily defined as ≥25 mmHg at rest, but revised during the 6th World Symposium on Pulmonary Hypertension in 2019.(3, 27)

The revision was based on a review of all available right heart catheterisation pressure values in healthy individuals.(16) However, the authors stressed that an isolated value does not characterise a clinical condition, nor does it describe the pathological process.(3)

Classification

The term PH encompasses a large group of heterogenous entities, and has therefore been subdivided by the WHO into 5 groups based on aetiology and clinical features.

Group 1 is known as pulmonary arterial hypertension (PAH), which is further divided into 7 subgroups. PAH is defined by pre-capillary PH, with mPAP ≥20 mmHg, pulmonary artery wedge pressure (PAWP) of ≤15 mmHg, as well as a component of increased pulmonary vascular resistance (PVR) of ≥3 Wood units. The aetiologies vary, but all create conditions of chronically raised PVR leading to progressive and severe RV dysfunction and failure.(3, 14)

Group 2 includes PH with underlying causes due to left heart pathology such as valvular lesions and left sided cardiac failure. This, in turn, leads to increased left atrial pressures and isolated post-capillary PH (although a combination of pre- and post-capillary can occur).(3, 21)

TABLE 2 **Updated clinical classification of pulmonary hypertension (PH)**

1 PAH
- 1.1 Idiopathic PAH
- 1.2 Heritable PAH
- 1.3 Drug- and toxin-induced PAH (table 3)
- 1.4 PAH associated with:
  - 1.4.1 Connective tissue disease
  - 1.4.2 HIV infection
  - 1.4.3 Portal hypertension
  - 1.4.4 Congenital heart disease
  - 1.4.5 Schistosomiasis
- 1.5 PAH long-term responders to calcium channel blockers (table 4)
- 1.6 PAH with overt features of venous/capillaries (PVOD/PCH) involvement (table 5)
- 1.7 Persistent PH of the newborn syndrome

2 PH due to left heart disease
- 2.1 PH due to heart failure with preserved LVEF
- 2.2 PH due to heart failure with reduced LVEF
- 2.3 Valvular heart disease
- 2.4 Congenital/acquired cardiovascular conditions leading to post-capillary PH

3 PH due to lung diseases and/or hypoxia
- 3.1 Obstructive lung disease
- 3.2 Restrictive lung disease
- 3.3 Other lung disease with mixed restrictive/obstructive pattern
- 3.4 Hypoxia without lung disease
- 3.5 Developmental lung disorders

4 PH due to pulmonary artery obstructions (table 6)
- 4.1 Chronic thromboembolic PH
- 4.2 Other pulmonary artery obstructions

5 PH with unclear and/or multifactorial mechanisms (table 7)
- 5.1 Haematological disorders
- 5.2 Systemic and metabolic disorders
- 5.3 Others
- 5.4 Complex congenital heart disease

PAH: pulmonary arterial hypertension; PVOD: pulmonary veno-occlusive disease; PCH: pulmonary capillary haemangiomatosis; LVEF: left ventricular ejection fraction.

Table 1: Updated clinical classification of pulmonary hypertension from the 6th World Symposium on Pulmonary Hypertension in 2019.(3)

Group 3 is PH due to pulmonary pathology such as chronic obstructive pulmonary disease (COPD), interstitial lung disease (ILD), or conditions which lead to hypoxia, such as obstructive sleep apnoea. Destruction of lung parenchyma, persistent or repeated pulmonary vasoconstriction, and vessel de-recruitment create pre-capillary PH.(3, 27)

Group 4 relates to chronic thromboembolic phenomena, leading to repeated occlusion of pulmonary vasculature and vascular remodelling.(28)

Group 5 relates to those cases of PH in which the cause of the raised mPAP is either not determined, or deemed to be multifactorial. There are 4 subgroups including haematologic, metabolic, fibrosing, and cardiac aetiology.(3, 27)Alternative, or complementary, classifications have been proposed based on haemodynamic features of PH. The basis for one such classification includes measures of PAWP, cardiac output, and PVR. Measurement of PAWP distinguishes pre-capillary PH (PAWP ≤ 15 mmHg) from post-capillary PH (PAWP ≥ 15 mmHg).(28, 29)

Group 1, or PAH, is relevant to this paper, and will be discussed in further detail.

Pulmonary Arterial Hypertension

PAH, as a subgroup of PH, is defined as mPAP ≥20 mmHg, PAWP of ≤15 mmHg, as well as PVR of ≥3 Woods units. As normal mPAP is ≤20 mmHg, some controversy remains regarding patients with mPAP of 20-25 mmHg. Previously, the term ‘borderline PAH’ was suggested, but this has fallen out of favour. What is clear, is that these patients are at an increased risk for the future development of PAH, and should be followed up closely.(30-32)

Although the true incidence of PAH is unknown, some European registries report rates of between 5 and 52 cases per 1 million population, making it a relatively rare condition.(33)

Due to the clinical complexity of studying the disease, epidemiological information has relied on the formation of registries. These are mostly found in high-income countries where resources are available to do so. The lack of data from developing and low-income countries affects our understanding of the burden of disease globally.(30)

In sub-Saharan Africa, the incidence is unclear. However, there is significant prevalence of conditions which may lead to PAH.(34)

Of the 25 million individuals affected by homozygous sickle cell disease (SCD) globally, more than half reside in Africa. PAH is an end-organ complication of SCD found in older individuals, mainly due to inflammatory and oxidative stress leading to pulmonary vessel endothelial dysfunction and subsequent increased mPAP. Of the 20-40% of SCD patients who develop PAH, 40% die within 40 months of diagnosis.(35)

Schistosomiasis is a common condition in many underdeveloped countries, and it has been suggested as the leading cause for Group 1 PH globally. A clear association exists between the schistosomiasis and PAH, through poorly understood mechanisms. A 2020 review article found that haemodynamic parameters as well as overall survival to be favourable in PAH due to schistosomiasis when compared to idiopathic PAH.(36)

Human Immune-deficiency (HIV) infection is also associated with an increased incidence of PAH, although the mechanism is again unclear. Importantly, the survival rate is reduced by half in patients with HIV who develop PAH. Although anti-retroviral therapy has a beneficial effect for these patients, the interaction between HIV related PAH and other conditions such as chronic lung disease due to tuberculosis (TB) and other viral infections likely raises the overall risk for PAH in the sub-Saharan population.(34, 37)

Importantly, there is significant overlap of these conditions amongst the population in sub-Saharan Africa, and the manner in which the incidence and severity of the illness is not fully understood.

When compared to other forms of PH, PAH affects individuals of a younger age, and a greater proportion of women are affected than men. Women in their middle-age are most susceptible.(38)

Pathophysiology of PAH

As previously shown, the following equation allows for an understanding of pulmonary haemodynamics:

mPAP = [right ventricle cardiac output (RVCO) x pulmonary vascular resistance (PVR)] + alveolar occlusion pressure.(1)

Numerous medical conditions exist which may lead to PAH by influencing the factors expressed in the above equation:

Increased PVR – The most significant mechanism resulting in the development PAH is a rise in PVR. This may occur as a result of occlusive vasculopathy with vasoconstriction, cell proliferation with fibrosis of vascular walls, conditions causing persistent occlusive microthrombosis, or conditions causing persistent or recurrent hypoxic vasoconstriction.(1, 17)

Increased RVCO – Generally, an isolated increase in pulmonary flow is easily compensated for by blood vessel recruitment in the vascular bed. However, in some situations, chronically increased pulmonary blood flow, or increased pulmonary venous pressure (represented by alveolar occlusion pressure), can lead to PAH.(1)

Increased pulmonary venous pressure can be caused by a variety of disorders including left-sided cardiac disease, constrictive pericarditis, and cardiac failure.

1	**Pulmonary arterial hypertension (PAH)**		
	1.1	Idiopathic PAH	
	1.2	Heritable PAH	
		1.2.1	BMPRII
		1.2.2	ALK1, ENG, SMAD9, CAV1, KCNK3
		1.2.3	Unknown
	1.3	Drug and toxin induced	
	1.4	Associated with:	
		1.4.1	Connective tissue disease
		1.4.2	HIV infection
		1.4.3	Portal hypertension
		1.4.4	Congenital heart diseases
		1.4.5	Schistosomiasis
1′	Pulmonary veno-occlusive disease and/or pulmonary capillary haemangiomatosis		
1″	Persistent pulmonary hypertension of the newborn (PPHN)		

Table 2: Classification of pulmonary hypertension group 1, pulmonary arterial hypertension.(14) PAH – pulmonary arterial hypertension; BMPRII – bone morphogenetic protein receptor type 2; ALK1 – activin receptor-like kinase type 1; ENG – endoglin; SMAD9 –

mothers against decapentaplegic homolog 9; CAV1 – caveolin 1; KCNK3 – potassium channel subfamily K member 3.

Idiopathic (group 1,1) and heritable (group 1,2) PAH are indistinguishable clinically. Heritable PAH (hPAH) is associated with specific gene mutations which display an autosomal dominant pattern of heritability.(14)

Certain drugs (group 1,3), such as some appetite suppressants, are known to cause PAH, while other prescription or over-the-counter medications are implicated but not yet proven. Mechanisms for PAH development are complex and varied between agents, and a high index of suspicion should be maintained in patients using these medications.(14)

Group 1.4 categorises other conditions which are commonly associated with the development of PAH.

A detailed description of the molecular pathophysiology in the development of PAH is beyond the scope of this paper, but ultimately all proposed and established mechanisms lead to an increase in pulmonary pressures, and thus, increased right heart pressures. A brief explanation is provided below.

Right Ventricle and Septum in Pulmonary Arterial Hypertension

Normal right heart physiology has already been discussed, and of significance is the RV sensitivity to increased PVR (Figure 1.).

PAH is characterised by an increase in RV afterload, which adapts through the mechanism of myocardial hypertrophy (right ventricular hypertrophy, RVH). RVH can maintain CO and compensate for increased afterload to a degree, but generally this is inadequate and will lead to RV failure (RVF) as the pathology progresses and RV afterload increases.(39)

RV adaptation to pathological states is complex and multifactorial. Some important factors include the type and severity of stress to the myocardium, the duration of the stress, and the age at which it occurs in an individuals’ life.

Further adaptation to the pathology is dependent on neurohormonal activation, the pattern of fibrosis and remodelling, and the alteration of gene expression.

All of these factors are interdependent, and are components of a web of interactions underlying the RV response to injury.(40)

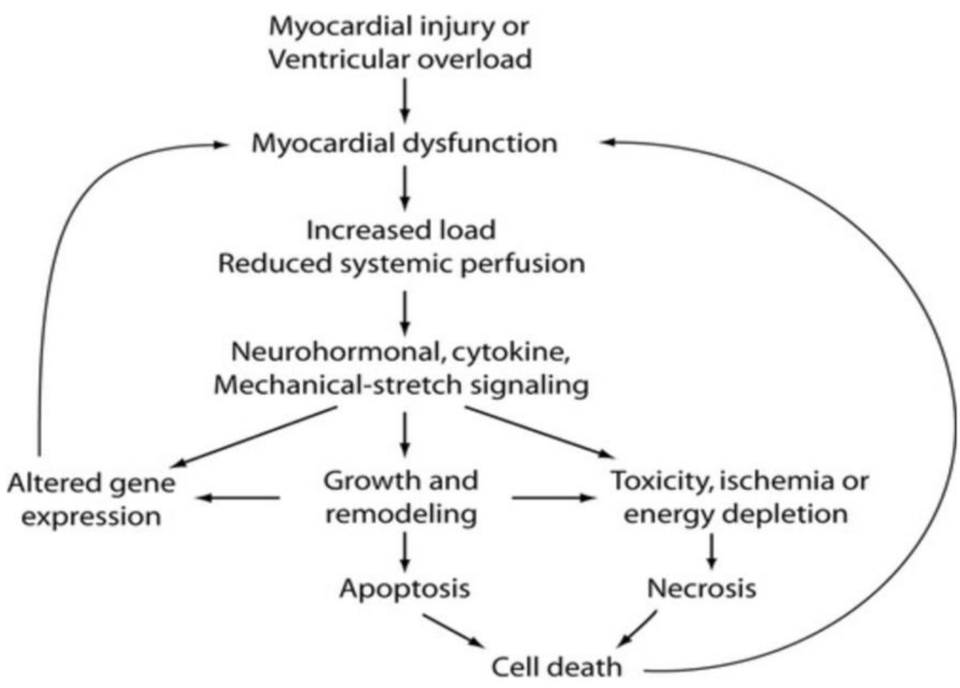

Figure 2. Proposed mechanisms and interactions between various factors influencing RV adaptation to stressors.(40)

Through these mechanisms, RV compensation for chronic pressure-overloaded states result in an increased density of myocardial connective tissue, an increased overall myocardial mass, and structural changes which affect haemodynamic functioning.(39, 40)

Partial adaptation is also achieved through homeometric (Anrep effect) and heterometric (Frank-Starling Law) cardiac autoregulation, within the limits of cardiac physiology. Homeometric adaptation of the RV has been demonstrated after pulmonary artery constriction, and relates to systolic function of the RV as quantified by the maximal elastance (eMax) of the RV.(41)

Despite these limited adaptive mechanisms, progressive RV dilation and dysfunction occur in PAH, and this is compounded by RV ischaemia which exacerbates RV failure and worsens CO. Activation of the endothelin system may play a significant role in the biomolecular pathogenesis of PAH, as demonstrated by the increased gene expression of endothelin-1 and endothelin-1 receptors, in monocrotaline-induced PAH in rodents.(40, 42)

Further neurohormonal activation, inflammatory mediators and oxidative stress, capillary loss and cell apoptosis result in progressive RV failure.(17, 41)

As previously mentioned, the RV dilation and pressure overload progressively push the septum leftward, which changes the RV and LV geometry. The general dimensions of the RV are increased, the LV begins to lose the normal cylindrical shape, and assumes a progressive "D" shape as seen in short-axis cross section. The septal dynamics and ventricular interdependence are also affected by the change in pressure and geometry. Patients with isolated volume overload tend to have the most marked D-shaped LV at end-diastole in the cardiac cycle, and a relatively spared geometry at end-systole. Patients with pressure-overload states tend to display abnormal geometry throughout the cycle, but the abnormality is accentuated at end-systole (Figure 3).(24, 43)

PRESSURE OVERLOAD *VOLUME OVERLOAD*

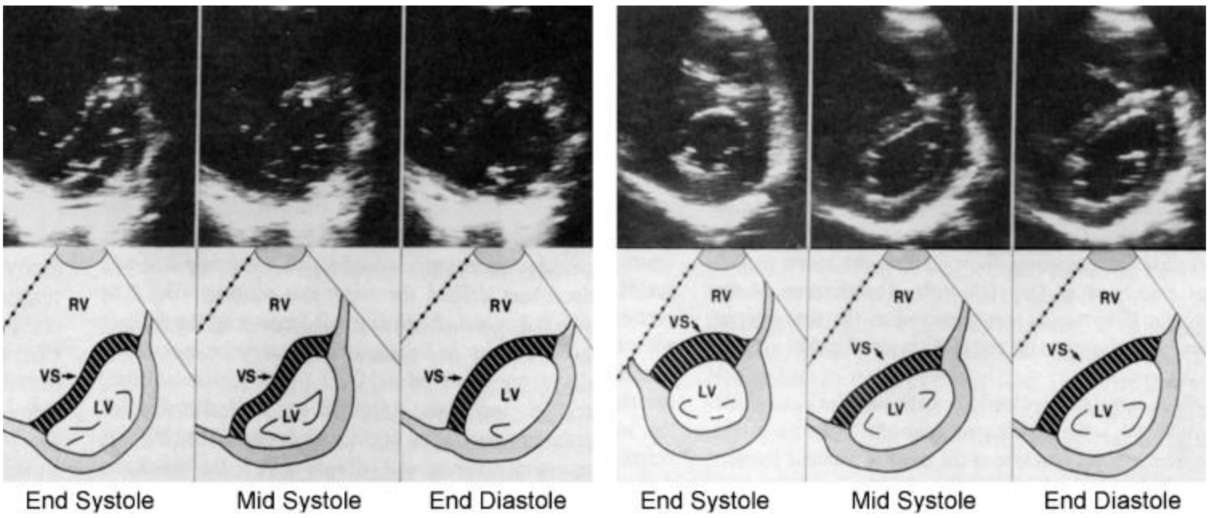

Figure 3. A series of short axis ultrasonographic views of the left ventricle and corresponding diagrammatic representations showing geometry of the LV in a patient with isolated RV pressure overload (3 panels on left side) and isolated RV volume overload (3 panels on right side), showing the respective LV deformation at the various stages of the cardiac cycle due to leftward shift of the septum.(43)

Once these changes start to occur, patients develop symptoms and signs of RVF from PAH. However, the onset is insidious.

DIAGNOSIS OF PAH

Diagnosis often occurs late in the clinical course of the illness due to a lack of symptoms early on, as well as significant difficulties in the availability of practical screening tools. Often a diagnosis is only made at a point where the disease has progressed substantially.(6)

This is a significant barrier, as early diagnosis of PAH is correlated with much better clinical outcome, improved quality of life, as well as long term survival. It is therefore reasonable to screen populations who are at risk of PAH. Currently, using multiple non-invasive screening tools in concert increases their predictive value. Thereafter, right heart catheterisation (RHC) is necessary for diagnosis of PAH.(6)

Symptoms typically include those of RVF, including exertional dyspnoea, malaise, fatigue, angina, syncope and pre-syncope, as well as fluid retention, pedal oedema, and ascites. These features are progressive, and may prompt a patient to seek healthcare. Clinical features in keeping with PH and RVF may be found on physical examination, prompting bedside tests including resting electrocardiography and echocardiography. This enables the probability of PH to be estimated.(44, 45)

Further investigation for the presence and cause of PH may include referral to a specialist centre where specific imaging, right-heart catheterisation, and genetic testing may be done as appropriate. This process is not straightforward, and often involves a multidisciplinary, and resource-intensive approach (Figure 4).(27)

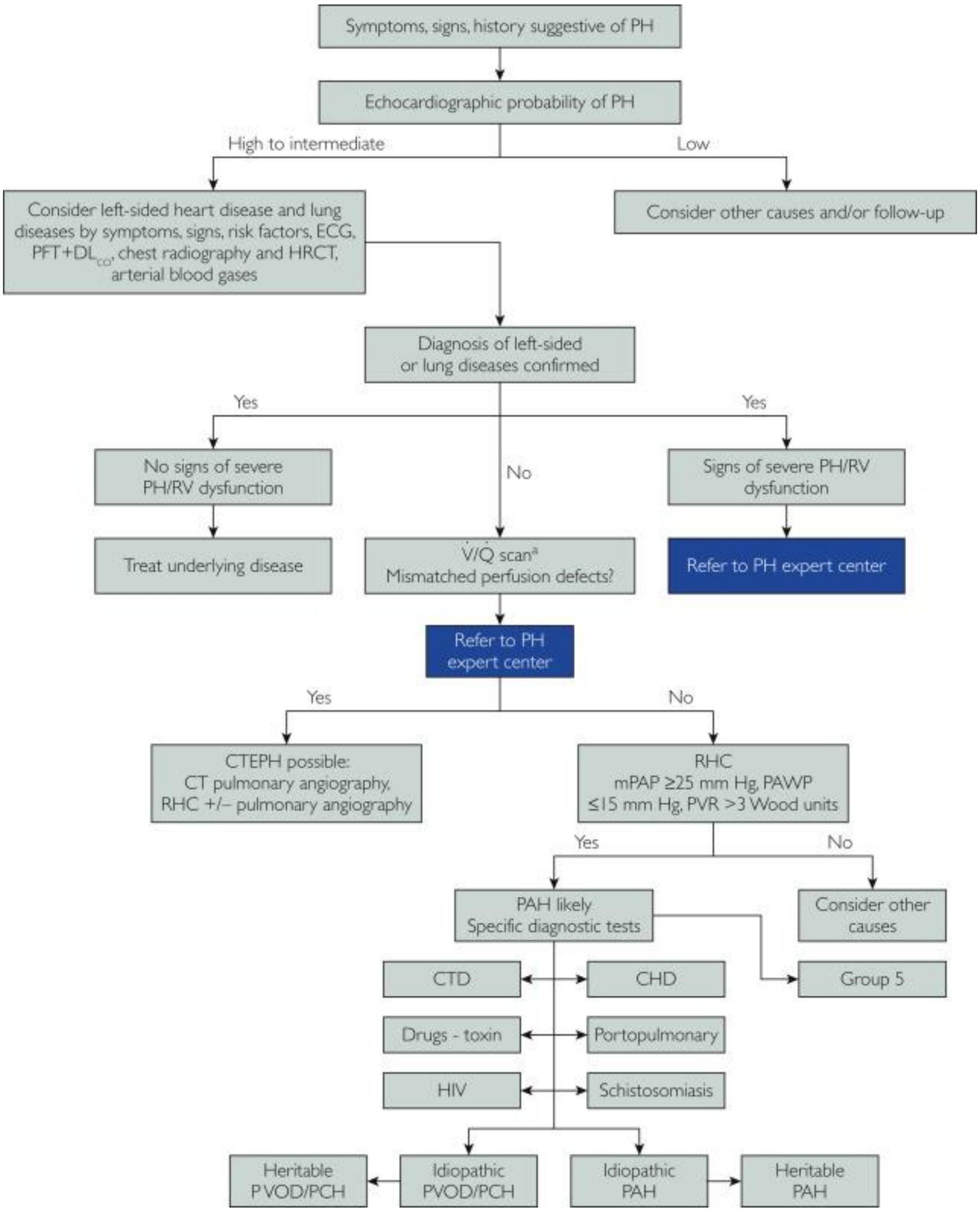

Figure 4. European Society of Cardiology/European Respiratory Society algorithm for the diagnosis of pulmonary hypertension. PH – pulmonary hypertension; ECG – electrocardiogram; PFT – pulmonary function tests; DL_{CO} – pulmonary carbon monoxide diffusing capacity; HRCT – high-resolution computed tomography; RV – right ventricle; V/Q – ventilation/perfusion ratio; CTEPH – chronic thromboembolic pulmonary hypertension; CT – computed tomography; RHC – right heart catheterisation; mPAP – mean pulmonary artery pressures; PAWP – pulmonary artery wedge pressure; PVR – pulmonary vascular resistance; PAH – pulmonary arterial hypertension; CTD – connective tissue disease; CHD – congenital heart disease; HIV – human immunodeficiency virus; PVOD – pulmonary veno-occlusive disease; PCH – pulmonary capillary haemangiomatosis.(45)

Although right-heart catheterisation remains the gold standard for diagnosis of PH and accurate measurement of pulmonary pressures, this investigation is invasive, and exposes patients to procedural risks as well as radiation.(31)

In contrast, transthoracic echocardiography is far more widely available as a safe bedside investigation, and therefore plays an important role in risk quantification, diagnosis, prognostication, and measurement of response to treatment.

ULTRASONOGRAPHY

Ultrasonography has become ubiquitous in well-resourced healthcare, and is increasingly available in poorer settings. It is non-invasive and cost effective.(2) In addition, various modalities have been developed and increasingly used around the world.

From initial development of the medical technology in the 1950's, ultrasound has progressed significantly. Images of a structure or organ are obtained using sonic waves in the following way:

Firstly, an electroacoustic transducer converts electrical energy into mechanical waves. The waves propagate through tissue, and are reflected and refracted by tissue interfaces of differing densities.

The reflected waves are then received by either the same transducer, or other detectors. This mechanical energy in the form of sonic waves is converted to electrical impulses, and then into an image through processing equipment, for final display to the user.(46)

Although there have been significant and progressive leaps forward in the hardware involved in the production of ever-improving image quality, available software has also improved in leaps and bounds as computing power has expanded exponentially.

RV ASSESSMENT WITH ULTRASONOGRAPHY IN PH

Various measurements to assess the RV have been validated, including multiple tools for static morphological assessment, RV 2-dimensional and mono-dimensional systolic assessments, tissue doppler RV systolic assessment, RV diastolic function assessment, as well as pulmonary haemodynamic assessment.(47)

However, echocardiography is limited by a number of factors, and its usefulness as a stand-alone test for screening in PAH has been called into question. Nonetheless, it remains a key component in the screening algorithm for PAH (Figure 4), provides insight into RV function and pulmonary pressures, and can assist in ruling out secondary causes for PH.(47)

The geometry of the RV makes direct measurement of RV ejection fraction difficult. Indirect measurements are therefore used. Assessment of tricuspid regurgitation jet velocity (TRV) is used as the main parameter in screening for PAH, although many other measurements and derivations have been used. These include measurement of pulmonary artery acceleration time (PAAT).(6, 27)

Pulmonary Arterial Acceleration Time

PAAT is a useful independent indicator of pulmonary haemodynamics. Sampling is performed at the pulmonary outflow tract. Pulsed-wave doppler is used to measure acceleration time of the pulmonary flow, with the sample volume placed adjacent to the pulmonic cusp on the side of the RV. Mean pulmonary artery pressure is estimated using the equation mPAP = 79 – (0.6 x $PAAT_{[ms\}}$).(47, 48)

When the PAAT is less than 120 ms, it has been found that the adjusted formula, mPAP = 90 – (0.62 x PAAT) performs better.(43)

In humans, a PAAT of >130 ms is considered normal, but values of mPAP need to be corrected for an increased heart rate (HR). A value of <100 ms is considered abnormal, and indicates an increased mPAP, possibly indicative of PH.(47)

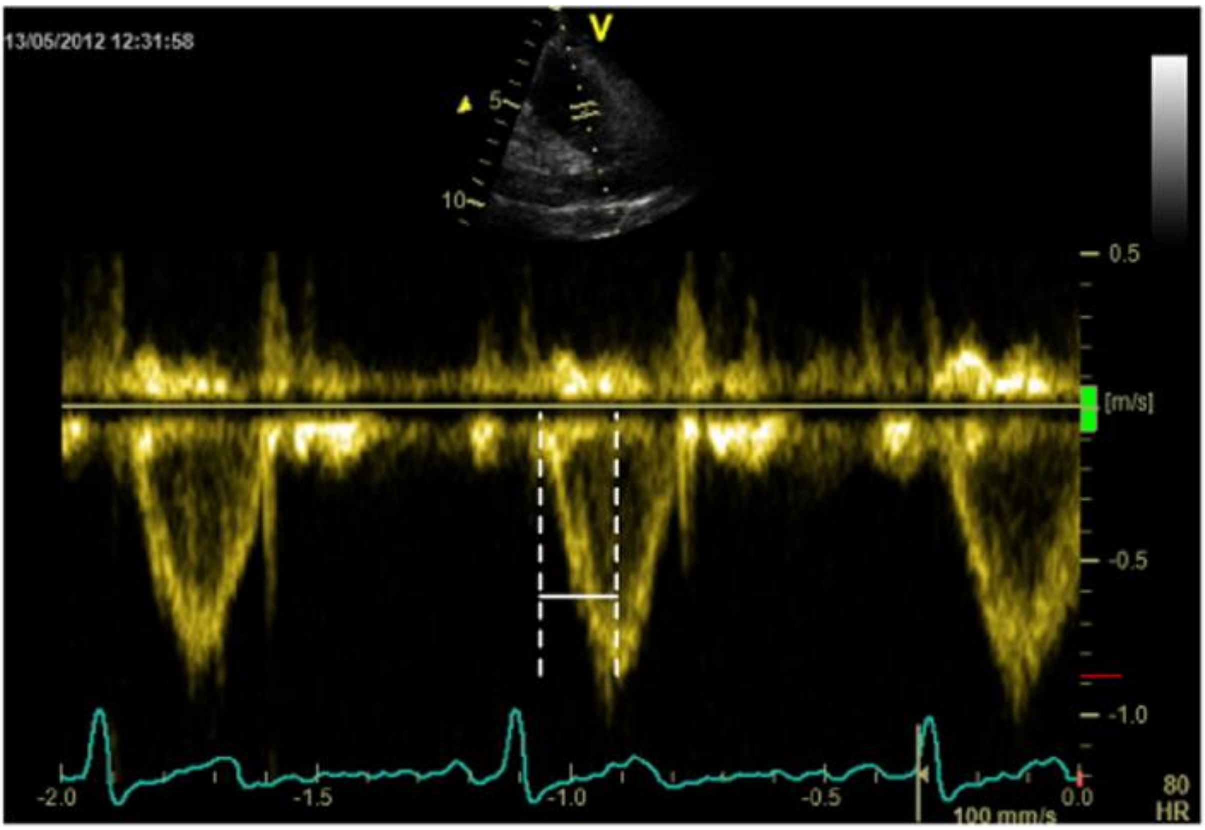

Figure 5. A typical pulsed-wave doppler ultrasonographic image of the right ventricular outflow tract showing pulmonary arterial acceleration time as measured between 2 dotted lines.(48)

In addition, the morphology of the flow wave may also indicate the presence of raised mPAP characterised by early or mid-systolic ‘notching’, which reflects increased pulmonary artery impedance, another characteristic of PH.(47-49)

Although the gold standard for measurement of pulmonary pressures is right heart catheterisation (12, 29, 44), PAAT has been validated as an indirect measure of mPAP. This validation enables the measurement of mPAP to be used in the diagnosis and monitoring of the response of PAH to treatment, obviating the need for repeated, invasive RH catheterisations.(43, 50, 51)

Other indicators of raised pulmonary pressure include echocardiographic measures of RV systolic pressures (RVSP) and RV diastolic pressures (RVDP). These are estimated using the modified Bernoulli equation of the peak tricuspid regurgitation jet velocity, where RVSP = $4V^2$ + right atrial pressure (RAP), and PADP = 4x (end-diastolic pulmonary regurgitant velocity)^2 + RAP. In the absence of any pulmonary valve abnormalities, RVSP is equal to systolic PAP (SPAP). In the setting of dyspnoea, a RVSP of greater than 40 mmHg qualifies for further investigation for PH, as per expert consensus of the American College of Cardiology Foundation and American Heart Association.(43, 48, 52)

Speckle Tracking Echocardiography

More recently, novel echocardiographic parameters have emerged as useful clinical tools in a variety of cardiac disorders. Myocardial deformation analysis uses speckle-tracking echocardiographic software to create strain patterns. These patterns may provide insight into right ventricular function in various pathological states, but the challenges associated with transthoracic echocardiographic imaging of the RV remain.(2, 10)

Although cardiac motion analysis can be done through traditional echocardiography, this is highly operator- and experience-dependent. Strain pattern analysis is useful in that it adds further objectivity and reliability to imaging of moving tissue.(53)

Basic Concepts

The term ‘strain’ reflects a fundamental property of materials, in that they can be deformed. In ultrasonography, various parts of an imaged structure move at different velocities, resulting in deformation which is quantifiable as a percentage of the original dimensions. An associated term is ‘strain-rate’, which describes the deformation over time.(53)

Although intuitive in some respects, strain is a complex mathematical concept which can be applied to objects of varying dimensions. For a one-dimensional object (1D), linear strain is defined by the formula:

$$\varepsilon = (L - L_0) / L_0 = \Delta L / L_0$$

where ε is strain, L_0 is baseline length, and L is length at measurement. This describes deformation along only a single axis, as reflected by “1D”. Strain is further divided into Lagrangian strain (where not only the initial and final measurements of L_0 and L are known, but also during the deformation process itself, or $\varepsilon_{(t)} = (L_{(t)} - L_{(t0)}) / L_{(t0)}$), and natural strain (in this instance, deformation is measured not against absolute values, but rather at a length at a previous time instance).

When further dimensions are added, such as in two-dimensional (2D) objects, there is deformation along 2 axes. In addition, the strain can be described as 'shear' deformation along both of these axes (where the upper and lower borders, and the left and right borders both move but at different velocities, and therefore deform in relation to each other). Therefore, 2D objects have 4 strain components – 2 strain, and 2 shear. Three-dimensional objects have 3 axes, and thus 3 strain components, and 6 shear strains, giving a total of 9 components.(53)

Development of Strain Pattern Analysis

Non-invasive myocardial strain measurements were pioneered using magnetic resonance imaging (MRI) in the late 1980's, and these concepts were translated to ultrasonography in the 1990's. Technology and software for tissue doppler imaging initially required post-processing of images to measure strain, but later allowed for real-time strain measurement as computing power increased.(54)

Today, although still primarily used as a research tool, the user-friendly nature of the imaging technique, improving processing power, and validation of various parameters for quantifying cardiac function, has paved the way for progressive adoption of these imaging techniques in clinical practice.(54)

Modalities – Tissue Doppler and Speckle-Tracking Echocardiography

Tissue doppler imaging allows for strain analysis by measuring tissue velocity parallel to ultrasound scan lines. This limits the modality to measurement of 1D strain measurement. It offers basic functional assessment of the LV unless multiple images are obtained and post-processing is applied.(54)

More advanced methods of feature tracking include speckle tracking echocardiography. This is dependent on the inhomogeneous acoustic features of the myocardium, which create varying acoustic densities, known as 'speckles' (appearing as small lighter areas). These have been found to correspond closely with tissue movement even though they do not represent actual tissue structure. Speckle tracking therefore allows for reliable measurement of the movement of structures of interest.(54)

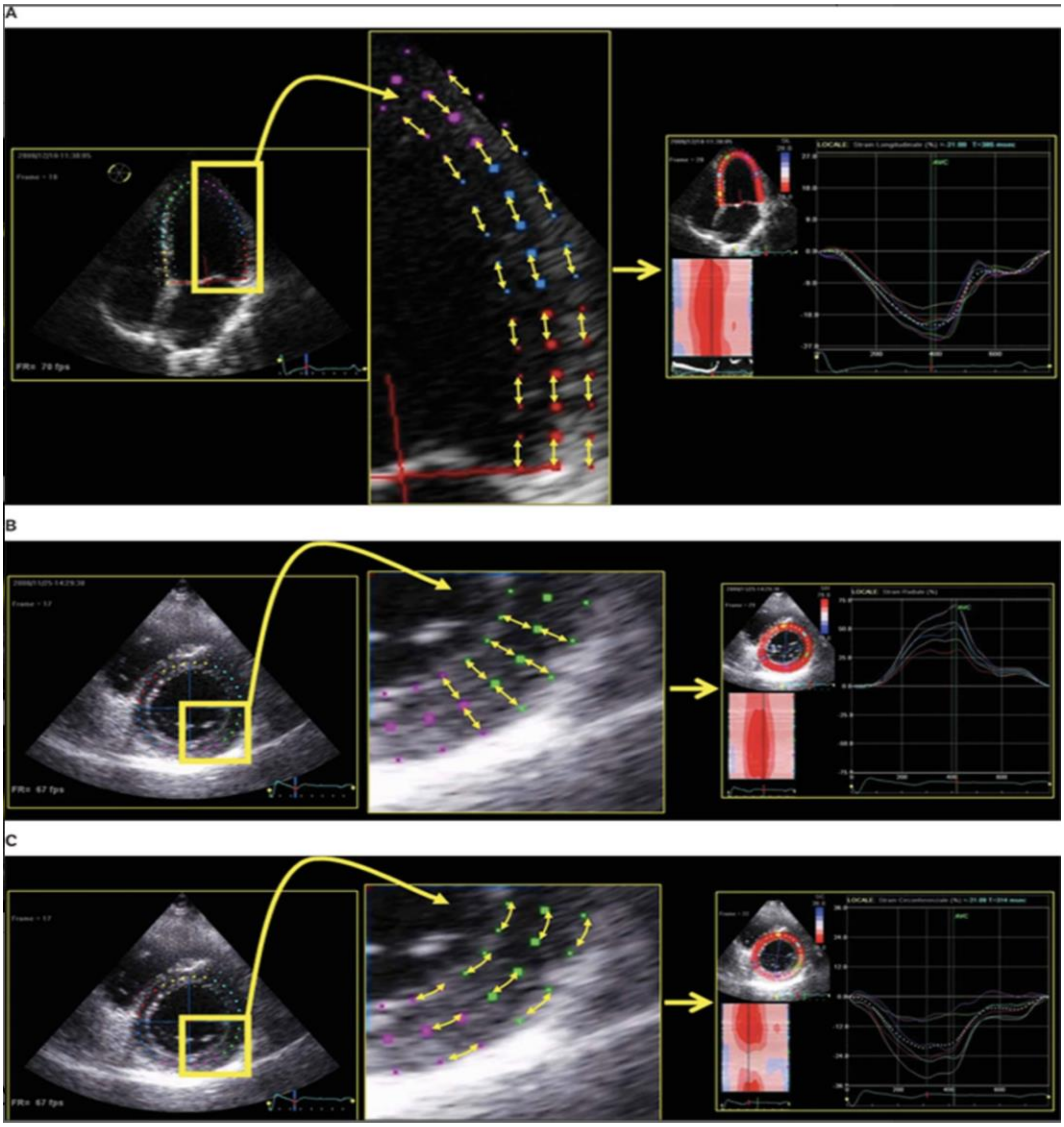

Figure 7. Speckle tracking analysis of ultrasound images of the heart. Panel A – parasternal long axis view, showing the greyscale image of the cardiac structures with acoustic ‘speckles’ visible in the left image, an enlarged segment of the image showing the axis (arrows) of deformation overlying the speckles in the middle image, and the associated strain pattern graph in the right image. Panels B and C show the same information for images of the heart in parasternal short axis views with radial strain pattern, and circumferential strain pattern, respectively.(55)

Often, software packages for speckle tracking are applied to regular greyscale ultrasound images during post-processing, and the automated image analysis has led to ease-of-use and reliability in 2D images.(54)

There are some limitations associated with the use of speckle tracking. Reliability is largely dependent on image quality, and may be significantly impaired by acoustic noise or other artefacts. Algorithms have been developed by various vendors to overcome these limitations to a degree, but these may impair sensitivity to subtle pathology. Accuracy of tissue doppler measurements depends on the orientation to acoustic signals, with a parallel beam yielding the most reliable measurements.(56)

Furthermore, the right ventricle has a complex morphology and dynamic function, which may confound the interpretation of strain patterns.

Despite the limitations, STE has been comprehensively validated as a method to assess multiple cardiovascular pathologies, including RV function in PH. cardiac MRI has shown high reliability for STE strain analysis, with low inter-observer variability. In addition, strain pattern analysis is more sensitive to early and subtle changes in LV function than ejection fraction (EF).(56-58)

Clinically, 3 components of myocardial deformation are described using STE, namely longitudinal strain (LS), radial strain (RS), and circumferential strain (CS). Due to the complex interwoven nature of the myocardium, individual fibres contribute to each of these components and selective assessment of cardiac layers is impractical. Strain rate (deformation over time) can offer a further tool in the assessment of cardiac function, but relies on a high temporal resolution, and is more accurate using tissue-doppler imaging.(54)

In addition, strain imaging can be applied to single or multiple segments of the heart, allowing for more directed analysis. This approach may be beneficial in that it reduces the need for obtaining optimal views of large portions of the heart for analysis.

Assessing Right Heart with Speckle Tracking Echocardiography

Assessment of any portion of the heart is possible, depending upon adequate image acquisition. This includes RV function, which is recognised as an important prognostic factor in PH. In children with PH, strain and strain rate imaging has been reliably used to quantify RV function, providing a complementary method to predict outcome.(59)

In one study comparing conventional echocardiographic indexes assessing RV function to 2D and 3D strain pattern analysis, found global longitudinal strain to correlate more closely with haemodynamics on right heart catheterisation.(60) Specifically, longitudinal strain of the RV has been established as a measure of RV function in PH.

Due to ventricular interdependence, as described above, right heart dysfunction can manifest as changes in left heart function, including that of the septal wall.

A 2016 study looking at echocardiographic features of the LV in children with PH found significant dysfunction of the LV on strain imaging when compared to healthy controls during cardiac catheterisation as investigation for PH. Segmental analysis found the reduced circumferential strain and strain rate to be most pronounced in the inter-ventricular septum in those children with PH.(61)

A further study examining LV strain using cMRI in 16 patients with PH, with 13 patients as control, found the most significant change in circumferential strain in the LV septal segment. In addition, literature shows a good association between global LV strain on cMRI, and STE. This supports the premise that PH with impaired LV function manifests as decreased septal circumferential strain.(62, 63)

Cardiac MRI is in itself a time-consuming, costly, and widely unavailable investigation, especially in resource-limited settings such as South Africa. As technology has improved, ultrasonography with STE may provide an invaluable tool in the screening for PH. Beyond screening and assessment for PAH, ultrasonography can be used to quantify severity of the disease, assess prognosis, and monitor response to treatment. 3-dimensional strain analysis, currently being refined, promises to be an even more powerful tool in the assessment of right heart function in PH. The importance of ultrasonography as an investigative tool for PH cannot be overstated.

EXPERIMENTAL PULMONARY ARTERIAL HYPERTENSION IN RODENTS

A rodent model with experimentally induced PH has been used extensively for research into diagnostic tools and novel treatments. The administration of monocrotaline (MCT) to rodents has been shown to provide a reliable development of severe PAH, with a predictable temporal course.(10)

The ideal PH model should manifest typical clinical features of the specific PH group being investigated, should display histological findings in keeping with those seen in humans, and should allow convenient and advanced investigation. Various animal models have been used, but all fall short of fulfilling the above criteria. This shortcoming is compounded by the fact that PAH is a heterogeneous entity in humans, with incompletely understood pathophysiology. Animal models may not reflect this complexity.(64)

Some advantages of using a rodent model include reliable reproducibility of pathology, genomic similarity to humans, relative economy, and shorter life spans.(64, 65) Multiple methods exist to induce PH in rodents. These include chronic exposure to hypoxic conditions, introduction of MCT, and surgical techniques such as pneumonectomy.(66)

Monocrotaline-Induced Pulmonary Arterial Hypertension

MCT is a plant-derived pyrrolizidine alkaloid which induces severe PAH when administered to rodents, as well as some other animals. It has been used for over 50 years to create experimental models of PAH, and its role in furthering our understanding and treatment of the disease is incalculable.(66, 67)

The toxin may be introduced by either subcutaneous or intraperitoneal injection, and produces PAH in a predictable, dose-dependent manner. The severity of PAH in rodents is also dependent on the age of the animal when administered.

MCT results in acute pulmonary artery injury by causing type II pneumocyte damage, precipitating microthrombosis, and inducing inflammatory cascades. These processes lead to a progressive pulmonary vasculopathy, severely increased pulmonary pressures, and death.(67)

The rodent-MCT model is however not perfect. The pathological process differs histologically from PAH in humans, as well as in the profile of plasma cytokines. In addition, MCT administration is accompanied by other organ involvement, most notably hepatic inflammation and microthrombosis. The effect of this pathology on the translatability of findings to humans is unclear.(67) Interestingly, toxic rape-seed oil ingestion by humans, such as occurred in Spain, matches most closely the pulmonary pathology seen with MCT in rodents.(67)

ULTRASONOGRAPHY IN RODENTS WITH PAH

As in humans, RHC remains the gold standard for measurement of pulmonary pressures in animal models; however, there are significant challenges related to this investigation in rodents. This has necessitated non-invasive measurements of RV function and PAP being developed and validated. Non-invasive techniques for assessment of PAP and RV include traditional ultrasonographic parameters used in humans.

As mentioned, PAAT is a clinically verified method of quantification of PH in humans, and its use has also been validated in rats. In a 2019 study by Zhu et al, a clear correlation was found between PAAT and RVSP measured by RHC in rats, and MCT- and hypoxia/Sugen-induced PAH.(2)

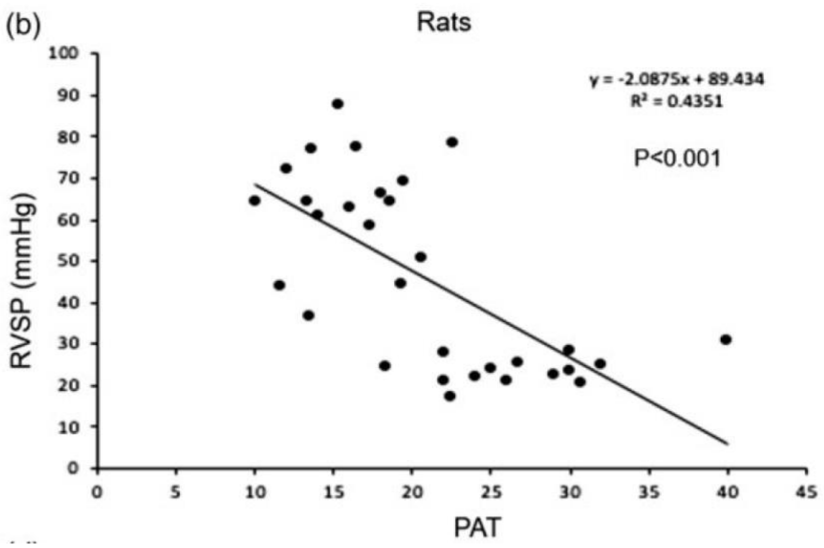

Figure 6. Graphical representation of the correlation between RVSP and PAAT (noted as ‘PAT’ on this graph) in rats with artificially-induced PAH.(2)

Multiple other studies have confirmed a strong correlation between PAAT and invasive measurement of pulmonary pressures in rodents, and its use in research as a reliable measure of pulmonary pressures is established.(68-70)

Beyond the traditional parameters, there is limited data available regarding STE of the right heart in rodent models. There has been growing interest in alternative methods of measurement of pulmonary pressures, especially as new technologies are being explored in clinical practice in humans.(10)

The functional relationship between the left and right heart is significantly and progressively disrupted by the development of right heart disease. Anatomically, the septal wall is shared between the left and right ventricles, and deformation of this portion of the myocardium is an inevitable consequence of right heart disease. However, there are no studies which describe the septal wall strain pattern in a rodent model with experimental PH.(71)

Most recently, Kimura et al. evaluated the right ventricle in rodents with MCT-induced right-ventricular heart failure (RVHF) using conventional ultrasonographic techniques, as well as strain-pattern analysis. A total of 26 rats were randomly assigned to either the RVHF or control groups. The researchers found clear RV dysfunction using conventional echocardiographic variables. Using strain pattern analysis, longitudinal and radial strain showed poor reproducibility, and only circumferential strain showed promise in evaluating the function of the right heart.(10) The researchers concluded that further investigation of circumferential strain pattern analysis of the septal wall is warranted. This technique may provide a promising tool in the ultrasonographic evaluation of PAH in rodents.

Septal Strain Analysis

In contrast to the RV free wall, the septum can be reliably visualised using transthoracic ultrasound, and strain-pattern analysis applied to the images. Available literature points to septal circumferential strain being a prominent indicator of PH with LV dysfunction. In addition, ultrasonography is relatively widely available, and automated or semi-automated strain pattern analysis is expected to become more accessible in the future.

Many staff members in emergency units and other areas of healthcare facilities are familiar with transthoracic echocardiography, and basic techniques are relatively easily taught. The investigation is noninvasive, and has negligible associated risk.

In light of these points, the validation of reduced septal wall circumferential strain as an indicator of PH in rodents could provide a stepping stone toward the eventual use as a screening tool in humans. This may obviate the need to obtain multiple measurements and images of the entire heart, and make screening widely available in the future. In addition, the septal wall circumferential strain pattern analysis can be correlated with a validated measure of pulmonary pressures, PAAT.

SECTION TWO - MANUSCRIPT

TITLE PAGE

Ultrasonographic circumferential strain pattern analysis of the cardiac septal wall in rodents with experimental pulmonary hypertension

Charl Francois Cornelis van Heyningen[1], Nkanyiso Hadebe[2], Marcelle Jagga[3]

[1,2,3] Department of Anaesthesiology and Perioperative Medicine, University of Cape Town and Groote Schuur Hospital, Cape Town, South Africa

ABSTRACT

Introduction

Pulmonary arterial hypertension (PAH) remains a devastating disease. Early diagnosis remains challenging, but is associated with improved outcomes. Rodent models have been extensively used to investigate PAH. Ultrasonographic strain pattern analysis provides a novel method of assessing cardiac function, but difficulties in transthoracic imaging of the right heart are a barrier to its use in diagnosis of PAH. Segmental strain pattern analysis of the intraventricular septum circumvents this problem while still providing insight into right ventricular (RV) function. In this paper, the authors compare the septal strain pattern of rodents with chemically-induced PAH, to a known indicator of right heart pressures, pulmonary arterial acceleration time (PAAT).

Method

This was a secondary analysis of ultrasonographic data of rodents from a previous study with chemically-induced PAH. Strain pattern analysis was used to identify peak circumferential strain (CS) of the septal segment on short axis views via transthoracic echocardiography. PAAT was also measured. Regression analysis was performed to assess the relationship between the parameters.

Results

The relationship between CS and PAAT was linear (y = 7.1343 + -0.6118 x, p=0.001, R^2 0.69). Rodents' predicted CS was equal to 0.59 + (-1.1 x $PAAT_{ms}$). CS increased by 1.1% for every 1 ms decrease in PAAT.

Conclusion

In rodents with PAH, peak CS of the septal segment on short axis view can be used to predict PAAT, and thus be used as a measure of PAH. Peak CS can reliably and easily be measured using transthoracic echocardiography, and may be valuable in the investigation and management of PAH in humans. Further studies should be conducted.

MANUSCRIPT

INTRODUCTION

The right heart is functionally complex, and difficult to assess. Many right heart (RH) pathologies have an insidious onset with non-specific symptoms. A multitude of special investigations exist, but with significant limitations including accessibility, low sensitivity, invasiveness and cost. These factors result in delayed diagnosis and treatment of right heart pathologies. This highlights the importance of finding effective, non-invasive measures of function of the right heart.(6)

One such disease is pulmonary arterial hypertension (PAH). The incidence is estimated to be between 10 and 52 cases per million (4). PAH carries a high mortality due to a variety of factors, including delayed diagnosis. Onset is subtle, with non-specific symptoms and clinical findings. Ultimately, diagnosis of PAH requires right heart catheterisation (RHC), and is defined by measured mean pulmonary arterial pressures of >20 mmHg at rest.(3, 12, 28)

Transthoracic echocardiography is extensively used in the workup and monitoring of PAH.(43) It is cost-effective and non-invasive(46), but is limited by the need for skilled operators using multiple parameters to assess RV function. Patients depend on efficient referral pathways to specialised centres, for access to this level of imaging.(45)

New software has allowed the development of novel ultrasonographic methods to assess cardiac function. These include speckle tracking echocardiography (STE) and strain pattern analysis. The benefits of this technology are that it requires relatively basic training, and is becoming more readily available.(55)

Limited data exists regarding strain pattern analysis in experimental PAH. A 2015 study analysing the entire right heart in rodents with experimental pulmonary hypertension showed promise in circumferential strain (CS) analysis of the RV as a measure of RH function. This analysis showed good correlation with other, validated echocardiographic features of pulmonary hypertension and right ventricular failure (RVF). However, the authors noted that reproducibility and diagnostic utility was limited, suggesting that further research be conducted.(10, 64)

One major limitation to the application of this technology is difficulty in imaging the right heart. This is overcome by selective segmental analysis of the septal wall, which is readily accessible even by novice transthoracic echocardiographers. Functional ventricular interdependence leads to septal wall motion abnormalities in PAH, which can by analysed using STE and compared to established echocardiographic measures of RV function. (22, 25, 41)

A rodent model with monocrotaline (MCT)-induced PAH and RVF is a well-established method for investigating this disease.(66) MCT injection has been shown to produce PAH in a predictable, time-dependent manner by induction of severe oxidative stress. Functional and structural changes in the RV have been confirmed via imaging such as cardiac magnetic resonance imaging (CMRI) and echocardiography, as well as through RHC and dissection of the heart.(67)

This study is a secondary analysis of ultrasound data gathered during research into the cardioprotective effects of various types of red wine on the development of experimental PAH in rats. The original study was performed at the University of Cape Town, South Africa, and published in 2018.(72)

In this paper, we aim to show the relationship between the circumferential strain of the septal wall segment and an established ultrasonographic measure of pulmonary hypertension, the pulmonary artery acceleration time (PAAT), in rodents with experimental PAH.

METHODS

Permission was granted by the authors of the original paper to make use of the existing animal data. Data collection took place from 05 December 2016 to 08 March 2017. A formal waiver for ethics approval was then obtained from the Animal Ethics Committee at the University of Cape Town Office of Animal Research Ethics (appendix A). For further details, please see the description of the relevant methodology in the original study (appendix B).

As this study was a retrospective analysis of existing data, a sample size was not calculated. In the original study, 35 male Long-Evans rats were used. All protocols complied with the care and use of laboratory animals guide published by the United States National Institute for Health, 2011. Rodents were randomised into the following groups: control rats (C), n=5, received only water; MCT rats (MCT), n=7, received only water and a subcutaneous injection of MCT; reduced-alcohol red wine (RARW) rats, n=5, received only reduced alcohol wine; MCT-treated rats (MCT+RARW), n=7, received daily reduced-alcohol wine and subcutaneous MCT; RW rats (RW), n=4, received only regular wine; MCT-treated rats (MCT+RW), n=7, received daily regular wine and subcutaneous MCT.

For the rodents randomised to MCT groups a single subcutaneous MCT injection took place on Day 0 at a dose of 80mg/kg. For all rodents, baseline ultrasonographic data was obtained 7 days prior to this (Day -7). Ultrasonographic data was again obtained 28 days after MCT administration of MCT (Day 28).To obtain ultrasound images, anaesthesia was induced using 4% isoflurane, and maintained with 2% isoflurane. Oxygen was used as the carrier gas at a flow rate of 1,5 l per minute delivered via nose cone. The rodents were placed supine, temperature maintained between 36,5°C and 37,5°C using a warm pad, and the chest shaved. Images were obtained using the VEVO 2100 Visualsonics, Inc. ultrasound machine (Toronto, Canada). LV short axis views were obtained, and pulmonary artery flow velocity was measured using pulsed-wave doppler. Multiple other parameters not relevant to this paper were also obtained. Ultrasound images and clips were stored locally on the password-protected hard drive of the ultrasound machine, and were only accessible to the authors of the original paper. Access was granted for the purpose of this study.Secondary analysis

Ultrasound images and clips were imported to a laptop computer for secondary analysis. Cardiac short axis ultrasound clips of the left ventricle (LV) were selected for each rodent. Selected clips included at least one full cardiac cycle recorded at the mid-papillary level. Clips were then exported to the VevoLab software suite (Visualsonics, Inc., Toronto, Canada), which allowed speckle tracking software to be applied to the endocardial border of the LV. Measures were taken to obtain the most effective tracking of the endocardial border, including use of the clips with the best view of the septum, careful selection of the points for tracking, and adjusting brightness to obtain optimal contrast.

The accuracy of speckle tracking was then assessed based on duration of effective tracking. Effective tracking was verified by a second observer. The quality of endocardial border speckle tracking was graded for each clip based on the percentage of the cardiac cycle where tracking was optimal. Clips where endocardium was tracked for 70% to 100% of the cycle were labelled ‘good quality’, between 50% and 70% were ‘poor quality’, and less than 50%, or those where tracking could not take place due to other factors were ‘very poor quality’.

On the LV short axis view, strain pattern analysis was used to measure the peak circumferential strain of the septum. Using the pulmonary artery flow velocity, the corresponding PAAT was measured, and all variables were tabulated on an Excel spreadsheet (Microsoft Excel, Microsoft Corporation, New Mexico, USA; www.microsoft.com).

Statistical Analysis

The sample size was determined by the sample size of the original study. Linear regression was performed using analysis of variance (ANOVA). Regression statistics were reported as multiple R, R squared, and adjusted R squared. Data was represented graphically as a scatter plot. Results were considered statistically significant at $P < 0.05$. Statistical analysis was performed using MedCalc® Statistical Software version 20.211 (MedCalc Software Ltd, Ostend, Belgium; https://www.medcalc.org; 2023). Regression analysis was performed on the entire dataset, as well as subsets with very poor quality traces removed, poor and very poor quality traces removed, and only high quality traces on day 28. Results for the entire data set, and for high quality data on day 28 were included.

RESULTS

A total of 52 ultrasound clips were available for measurement. 26 clips (50 %) were high quality, and the remainder (26 clips, 50 %) were either poor quality, very poor quality. Of the total clips, 37 were taken in rodents which had not received MCT, and did not have PHT. 15 clips were taken from rodents on day 28 after receiving MCT, and had established PHT.

1. Table 1 and 2 (see graphs and tables) shows the measured PAAT and CS values for all of the rodents. In those rodents that did not have PHT (n=37), mean PAAT was 21,41 ms (IQR: 20,62 to 24,24 ms), and mean CS was -22,85 % (IQR: -19,57 to -25 %). In those rodents with PHT (n=15), mean PAAT was lower at 14,18 ms (IQR: 12,75 to 15,23 ms)), and mean CS was increased at -13,05 % (IQR: -10,5 to – 18,59%).

2. Graph 1 (below) shows least squares linear regression of PAAT (dependent variable) vs. CS (independent variable) of the total data. The relationship was found to be linear, as described by the equation y = 12.9387 + -0.3323 x, p=0.001, R^2 0.31. CS decreased by 0.33 % for every 1 ms decrease in PAAT.

Graph 1: Least squares linear regression of PAAT (dependent variable) vs. CS (independent

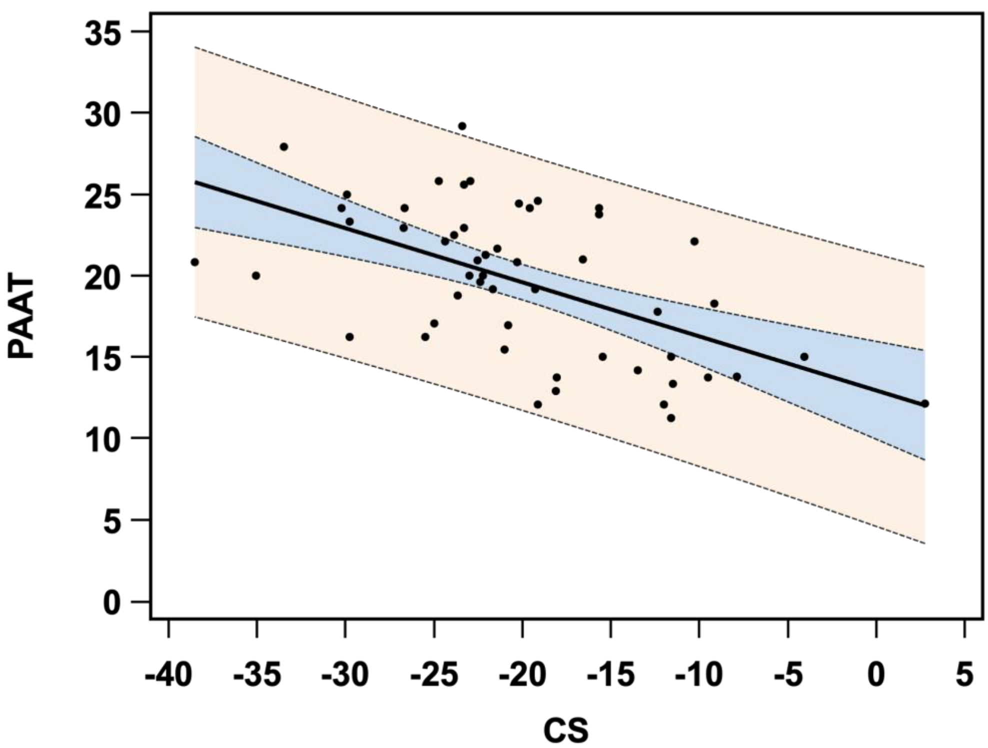

variable) of all data.

3. Table 3 displays the regression analysis for the total data.

4. Table 4 shows only high-quality data taken on day 28. A total of 26 high-quality clips were available. After exclusion of the high quality baseline (Day –7) clips, 11 high quality clips remained. 7 measurements were taken in rodents which had received MCT and had established PAH. Mean (SD) CS and PAAT values were -13,96 % (-11,75 to -20,66 %), and 14,55 ms (IQR: 13,78 to 19,3 ms) respectively.

5. Graph 2 shows least squares linear regression of the high quality data at day 28. PAAT was plotted as an independent variable against CS. The following equation was derived: y = 7.1343 + -0.6118 x , p=0.001, R^2 0.69. Rodents' predicted CS was equal to 0.59 + (-1.1 x $PAAT_{ms}$). CS increased by 1.1% for every 1 ms decrease in PAAT.

DISCUSSION

A rodent model with MCT-induced PAH and RVF is a well-established method for investigating this disease and appropriate for this study.(66) MCT injection has been shown to produce PAH in a predictable, time-dependent manner by induction of severe oxidative stress. Functional and structural changes in the RV have been confirmed via imaging such as CMRI and echocardiography, as well as through RHC and dissection of the heart.(67)

Traditional echocardiographic measurements of RV function are hindered by the inherent difficulty in obtaining views of the right heart due to a small echocardiographic window in rodents. In addition, measurements taken are angle-dependent. The use of STE overcomes this problem, but, as shown by Kimura et al, RV free wall imaging remains difficult.(10) Limiting STE analysis to the septal wall, and measuring only CS is comparably easy. This allows for relative novices to obtain views and apply STE software.

Main findings

The principal finding of this study is that peak CS of the septal wall predicts pulmonary artery pressures in rodents. For the given PAAT values, a linear relationship exists between CS and PAAT. Despite inherent difficulties in rodent echocardiography due to a limited transthoracic window and fast heart rate, our measurements showed good reproducibility. We also found that CS analysis could be performed quickly and easily using the VevoLab software suite.

Traditional Echocardiographic Variable - In those rodents that did not receive MCT, PAAT fell within the normal range. In those rodents that did receive MCT, PAAT decreased significantly by day 28. This confirmed development of PAH with RV failure using an established measure of right heart function. Our measurement of PAAT reflected results found in the original paper, which found mean PAAT = 24.43 ms ± 1.64 for controls (no MCT), and PAAT = 13.95 ms ± 0.95 for the MCT group. (72)

Speckle Tracking Echocardiography - STE analysis showed a significant reduction in CS of the septal segment of the myocardium in those rodents which received MCT, while CS was unchanged in those rodents that did not receive MCT. Regression analysis was performed on the entire data set, as well as the subset of high quality data on day 28. The subset analysis excluded all data points taken on day -7 (at which point none of the rodents had received MCT or had PAH), as well as the poor and very poor quality traces. The remaining 11 data points were high quality and included controls as well as rodents with varying degrees of established PAH. This was done to exclude excessive points in rodents which had normal PAAT and CS values, and traces which were unreliable due to poor or very poor tracking.

Both total data and subset analysis showed similar findings. Although the subset analysis had a greater R^2 value compared to the total data (0.69 vs 0.31 respectively), the confidence interval was much wider due to a smaller sample size.

No comparable studies exist in which only the septal wall peak CS is measured in rodents with PAH. The findings complement those of Kimura et al. Using a rodent model with MCT-induced PAH, their study examined multiple traditional echocardiographic variables of the right and left heart. Additionally, STE was used to analyse longitudinal, radial, circumferential, and transverse strain patterns, and RHC performed. The authors concluded that circumferential strain pattern analysis to evaluate RV function may be promising. The findings on CS were limited by a lack of reproducibility and impaired diagnostic utility and the authors added that further investigation was required.(10)

Traditional quantification of RV function has required imaging of the entire RV. Previous papers assessing the use of STE and strain pattern analysis have assessed multiple parameters, including circumferential strain of the entire RV. Significantly, we found that the CS of the septal wall alone can indicate the presence and degree of RV dysfunction. This negates the need for imaging of the entire RV.

A major strength of our study is that it showed a strong signal for the existence of a relationship between CS and RV function. This confirms the promise of a new parameter for measurement of PAH in humans, and further studies can be confidently undertaken. The use of genetically identical animal models under laboratory conditions allowed for the exclusion of confounding factors. This resulted in high-quality data for analysis and interpretation.

Our findings were limited by the following factors.

Firstly, the study was a secondary analysis, and the original study was not focused on viewing the septal wall. Therefore, we did not have any control over optimisation of septal wall imaging. Secondly, echocardiography of rodents is inherently challenging due to size of the anatomy, as well as the heart rate. In some clips, rib or sternal shadows obscured views of the septum for part, or all of the cardiac cycle. In these cases, software tracking of the septal wall was only possible when the septal wall was visible, or was not possible at all. Although data collection was less dependent on operator skill than traditional ultrasound parameters, this was still a factor.

In those clips where the quality of the image was compromised for reasons mentioned above, software tracking of the endocardial border was impaired to varying degrees. This necessitated the grading of the quality of the software tracking for subset analysis. Exclusion of these clips resulted in a decreased sample size and a wider confidence interval.

Thirdly, we could not compare septal CS to the gold standard for measurement of pulmonary pressure, namely RHC. However, PAAT is a validated measure of RV function, and is traditionally used in experimental PAH to quantify RV function. Lastly, we are unable to assess whether CS and PAAT maintain a linear relationship at values beyond the range of data points available to us. It may be possible that CS no longer predicts PAAT at more extreme measures.

This led to poor or absent visualisation of the septal wall in some clips. Ultrasonographic views obtained in the original study were not necessarily optimal for viewing the septal wall, which was another contributing factor to the exclusion of some clips.

Future studies should be designed to further investigate our findings, as well as address the limitations of our study. This could provide more insight into the relationship between PAAT and CS. Human trials could be conducted at specialised PH centres, and septal wall CS measurements could be taken at the time of RHC.

Conclusions

Our findings show that septal wall CS can be used to evaluate RV function in rodents with experimental PAH. This has important implications for future research using rodents. If validated in humans, the clinical applications would be significant. In future, septal wall CS could become a fast, readily available and non-invasive screening tool for PH by non-specialist clinicians.

GRAPHS AND TABLES

Table 1 – All Data (rodents did not receive MCT)

	Day -7		Day 28	
RODENT LABEL	PAAT (ms)	CS (%)	PAAT (ms)	CS (%)
1.1	20,83	-38,52	No second measurement	
1.2	19,58	-22,4	21,67	-21,4
1.5	24,17	Unable to track	15	-15,46
2.2	24,17	-30,25	19,17	-19,26
2.4	22,92	-23,29	20,95	-22,52
2.5	22,5	-23,86	20,83	-20,31
2.6	25,83	-22,93	25,83	-24,75
2.8	27,92	-33,48	22,08	-24,38
3.3	24,17	-15,66	18,3	-9,13
3.4	21,25	-22,09	21	-16,6
3.5	29,17	-23,4	16,25	-29,75
3.9	24,58	-19,15	No second measurement	
3.12	17,08	-25	12,92	-18,13
MEAN	23,398	-25,00	19,45	-20,15

Table 2 – All Data (Rodents received MCT)

	Day -7 (No PHT)		Day 28 (PHT)	
RODENT LABEL	PAAT (ms)	CS (%)	PAAT (ms)	CS (%)
1.3	22,08	-10,27	13,75	-9,51
1.4	22,5	Unable to track	12,08	-12,01
1.6	24,17	-26,68	13,33	-11,48
1.7	24,44	-20,18	15,45	-21,01
2.1	20	-23,01	13,81	-7,89
2.3	22,93	-26,7	14,17	-13,5
2.7	24,17	-19,57	17,78	-12,37
2.9	18,75	-23,64	15	-11,62
3.1	19,17	-21,69	11,25	-11,59
3.2	20	-22,22	12,11	2,76
3.6	25,56	-23,3	16,25	-25,5
3.7	23,33	-29,79	13,75	-18,05
3.8	23,75	-15,69	16,96	-20,81
3.10	20	-35,07	12,08	-19,13
3.11	25	-29,92	15	-4,07
MEAN	22,39	-23,41	14,18	-13,05

Table 3 -

Regression Analysis of All Data

Dependent Y	PAAT
Independent X	CS

Least squares regression

Sample size	52
Coefficient of determination R^2	0.3149
Residual standard deviation	3.8822

Regression Equation

y = 12.9387 + -0.3323 x

Parameter	Coefficient	Std. Error	95% CI	t	P
Intercept	12.9387	1.4935	9.9388 to 15.9386	8.6630	<0.0001
Slope	-0.3323	0.06931	-0.4715 to -0.1931	-4.7942	<0.0001

Analysis of Variance

Source	DF	Sum of Squares	Mean Square
Regression	1	346.4120	346.4120
Residual	50	753.5806	15.0716

F-ratio	22.9844
Significance level	P<0.0001

Residuals

Shapiro-Wilk test for Normal distribution	W=0.9735 accept Normality (P=0.2956)

MedCalc® Statistical Software version 20.211 (MedCalc Software Ltd, Ostend, Belgium; https://www.medcalc.org; 2023)

Table 4 - High Quality Data from Day 28			
RODENT LABEL	PAAT (ms)	CS (%)	RECEIVED MCT
1.5	15	-15,46	No
2.5	20,83	-20,31	No
2.6	25,83	-24,75	No
2.8	22,08	-24,38	No
1.3	13,75	-9,51	Yes
1.4	12,08	-12,01	Yes
1.6	13,33	-11,48	Yes
1.7	15,45	-21,01	Yes
2.1	13,81	-7,89	Yes
2.3	14,17	-13,5	Yes
2.7	17,78	-12,37	Yes

Table 5 -

Regression Analysis of High Quality Data on Day 28

Dependent Y	PAAT_3
Independent X	CS_3

Least squares regression

Sample size	11
Coefficient of determination R^2	0.6921
Residual standard deviation	2.5572

Regression Equation

y = 7.1343 + -0.6118 x

Parameter	Coefficient	Std. Error	95% CI	t	P
Intercept	7.1343	2.2702	1.9989 to 12.2698	3.1426	0.0119
Slope	-0.6118	0.1360	-0.9195 to -0.3041	-4.4974	0.0015

Analysis of Variance

Source	DF	Sum of Squares	Mean Square
Regression	1	132.2663	132.2663
Residual	9	58.8524	6.5392

F-ratio	20.2268
Significance level	P=0.0015

Residuals

Shapiro-Wilk test for Normal distribution	W=0.9806 accept Normality (P=0.9694)

MedCalc® Statistical Software version 20.211 (MedCalc Software Ltd, Ostend, Belgium; https://www.medcalc.org; 2023)

Graph 2

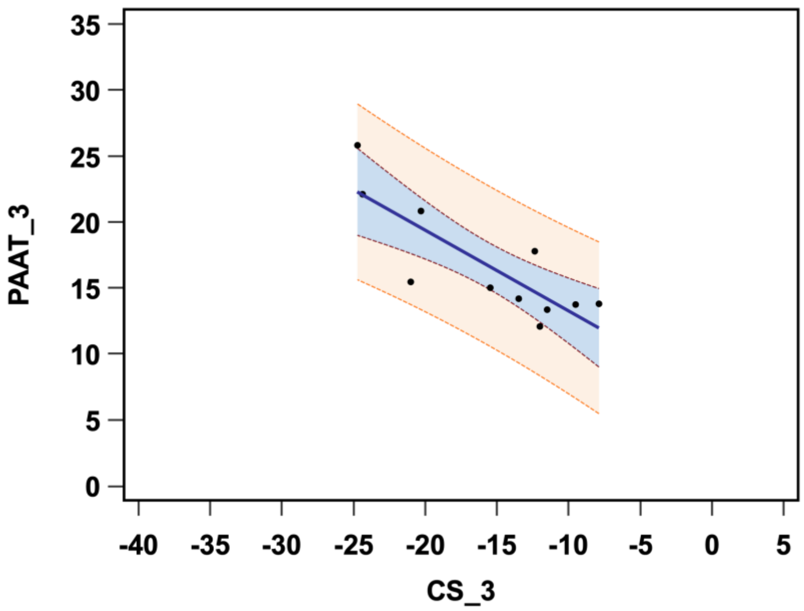

Least squares linear regression of PAAT (dependent variable) vs. CS (independent variable) of high quality clips of rodents at Day 28.

SECTION THREE

SEPTAL STRAIN PATTERN IN EXPERIMENTAL PULMONARY HYPERTENSION

APPENDIX A – AEC AUTHORISATION LETTER

UNIVERSITY OF CAPE TOWN
Faculty of Health Sciences
Animal Ethics Committee

Room G50 Old Main Building
Groote Schuur Hospital
Observatory 7925
Website: www.health.uct.ac.za/fhs/research/animalethics/forms

30 November 2020

Dr Nkanyiso Hadebe and Dr Marcelle Jagga
Department of Anaesthesia
Faculty of Health Sciences
University of Cape Town

Dear Dr Nkanyiso Hadebe and Dr Marcelle Jagga

PROTOCOL TITLE: Circumferential Strain Analysis of Septal Wall As A Novel Indicator Of Pulmonary Hypertension In Rodents (MMed Candidate- CFC van Heyningen)
FHS AEC REF NO: 021_004

Thank you for submitting your amended protocol to the Faculty of Health Sciences (FHS) Animal Ethics Committee (AEC) for review.

I am pleased to inform you that the FHS AEC has **authorised** your protocol, which will terminate on **31 May 2024.**

Number of animals & species: N/a (existing data linked to AEC REF. 016_001)

Please quote the FHS AEC REF NO (above) in all future correspondence.

Please note that the authorisation of this protocol imposes the following obligations on the principal investigator (PI):

1. To submit an annual mandatory progress report. The first annual report for this protocol is due on **28 February 2022**. The forms can be accessed from http://www.health.uct.ac.za/fhs/research/animalethics/forms
2. To submit a final mandatory report on the **31 May 2024**, please access the final report form from: http://www.health.uct.ac.za/fhs/research/animalethics/forms
3. Ensuring that all study participants perform within the confines of the procedures and experimental design of the protocol as authorised, or as amended.
4. Ensuring that all study participants comply with all applicable national legislation, UCT policies, FHS AEC policies and standard operating procedures (SOPs) and national standards (SANS 10386: 2008).
5. Ensuring compliance with DAFF Section 20 requirements.

AEC REF# 021_004

6. Ensuring that you as the PI immediately alert the FHS AEC to any event involving the welfare of the animals which has occurred during the course of the study, as well as the actions that were taken to respond to these events.
7. Ensuring that you as the PI alert the FHS AEC to any new or unexpected ethical issues that arose during the course of the study, and how these issues were addressed.
8. Ensuring that all study participants are registered with or have been authorised by the South African Veterinary Council (SAVC) to perform the procedures on animals or will be performing the procedures under the direct and continuous supervision of SAVC-registered veterinary professionals or SAVC-registered para-veterinary professionals.
9. If the PI or any study participant is in any way uncertain how to respond to any of these obligations or deal with any of the issues referred to above, they must consult with FHS AEC.
10. All animals found dead must be reported to the RAF on the appropriate form: http://www.health.uct.ac.za/fhs/research/animalethics/forms
11. All animals found in distress must be reported to the RAF on the appropriate form.

My best wishes for a successful research and /or teaching endeavour.

Yours sincerely

PROF G. LOUW
CHAIR, FHS AEC

AEC REF# 021_004

APPENDIX B – ORIGINAL STUDY METHODOLOGY

METHODS

Animal Group

The study was approved by the Faculty of Health Sciences Animal Ethics Committee, University of Cape Town (ethics number 016/001). All protocols were carried out in compliance with the care and use of laboratory animals guide published by the United States National Institute for Health in 2011. Male Long Evans rats weighing 150-175g were housed in the Faculty of Health Science Animal Unit at the University of Cape Town, in a 12-hour dark/light cycle with room temperature between 20 ◦C and 23 ◦C and humidity maintained at 40%. A maximum of 3-4 rats were housed per cage. The drinking water of the rats was supplemented with one part of either 5.5% reduced-alcohol or 15% regular red wine to seven parts of water, mimicking an amount equivalent to 2-3 glasses of wine per day in humans, as previously described (29). The groups were pre-treated with wine or water for 7 days before receiving a single injection of MCT (80mg/kg subcutaneous, see Figure 1). The following randomised groups of rats were used: control rats (C), n=5, received only water; MCT rats (MCT), n=7, received only water and an injection of MCT; RARW rats, n=5, received only reduced-alcohol wine; MCT-treated rats (MCT+RARW), n=7, received daily reduced-alcohol wine; RW rats, n=4, received only regular wine; MCT-treated rats (MCT+RW), n=7, received daily regular wine.

The total duration of the study was 35 days, which included 7 days of pre-treatment with reduced-alcohol wine, regular wine, or water, and 28 days following MCT-induced PAH injection. Echocardiography was performed on all the rats on day -7 and again on day 28 (Figure 2). The stability of the wine was tested during the experimental period twice a week for 4-weeks. After the 28 days, the animals were anaesthetised, blood samples were collected by cardiac puncture, biometric measurements were carried out and the hearts were separated into right ventricle (RV) and left ventricle (LV) plus septum for histology, as previously described (34).

Echocardiography

For echocardiography, the rats were anaesthetised with 4% isoflurane gas, to induce deep unconsciousness which was maintained with 2% isoflurane via nose cone delivery, with oxygen at a flow rate of 1.5L/minute. Rats were reclined in a dorsal position and secured to a warm pad to keep their body temperature between 36.5 ◦C and 37.5 ◦C. The tail was covered to reduce heat loss. The chest was shaved, and a warm ultrasound gel was applied. The following parameters were measured: diastolic thickness of RV from a long and short axis view, pulmonary artery acceleration time (PAAT), peak flow from the pulmonary artery, and A and E waves as well as tricuspid annular plane systolic excursion (TAPSE) from a 4-chamber apical view using VEVO 2100 Visualsonics, Inc.

ACKNOWLEDGEMENTS

Nkanyiso Hadebe, for your guidance and mentorship, as well as introducing me to the field of animal research.

Marcelle Jagga, for your support and help with the initial stages of writing this thesis.

Professor Robert Dyer for your invaluable input and guidance before submission of the thesis.

Professor Jeff Coetzee for your assistance with the statistical analysis of the data.

Professor Justiaan Swanevelder for your support and encouragement over the course of this research.

FUNDING

No funding was required, as the study utilised existing data.

References

1. Chamarthy MR, Kandathil A, Kalva SP. Pulmonary vascular pathophysiology. Cardiovasc Diagn Ther. 2018;8(3):208-13.
2. Zhu Z, Godana D, Li A, Rodriguez B, Gu C, Tang H, et al. Echocardiographic assessment of right ventricular function in experimental pulmonary hypertension. Pulm Circ. 2019;9(2):2045894019841987.
3. Simonneau G, Montani D, Celermajer DS, Denton CP, Gatzoulis MA, Krowka M, et al. Haemodynamic definitions and updated clinical classification of pulmonary hypertension. Eur Respir J. 2019;53(1).
4. Hoeper MM, Simon RGJ. The changing landscape of pulmonary arterial hypertension and implications for patient care. Eur Respir Rev. 2014;23(134):450-7.
5. Benza RL, Miller DP, Barst RJ, Badesch DB, Frost AE, McGoon MD. An evaluation of long-term survival from time of diagnosis in pulmonary arterial hypertension from the REVEAL Registry. Chest. 2012;142(2):448-56.
6. Lau EM, Humbert M, Celermajer DS. Early detection of pulmonary arterial hypertension. Nat Rev Cardiol. 2015;12(3):143-55.
7. Bossone E, D'Andrea A, D'Alto M, Citro R, Argiento P, Ferrara F, et al. Echocardiography in pulmonary arterial hypertension: from diagnosis to prognosis. J Am Soc Echocardiogr. 2013;26(1):1-14.
8. Bazan IS, Fares WH. Pulmonary hypertension: diagnostic and therapeutic challenges. Ther Clin Risk Manag. 2015;11:1221-33.
9. Muntean I, Benedek T, Melinte M, Suteu C, Togãnel R. Deformation pattern and predictive value of right ventricular longitudinal strain in children with pulmonary arterial hypertension. Cardiovasc Ultrasound. 2016;14(1):27-.
10. Kimura K, Daimon M, Morita H, Kawata T, Nakao T, Okano T, et al. Evaluation of right ventricle by speckle tracking and conventional echocardiography in rats with right ventricular heart failure. Int Heart J. 2015;56(3):349-53.
11. Beppu S, Izumi S, Nagata S, Park YD, Masuda Y, Sakakibara H, et al. [Ventricular interdependence reflected in interventricular septal motion: with special reference to right ventricular pressure overload]. J Cardiogr Suppl. 1984(3):53-62.
12. Hoeper MM, Bogaard HJ, Condliffe R, Frantz R, Khanna D, Kurzyna M, et al. Definitions and diagnosis of pulmonary hypertension. J Am Coll Cardiol. 2013;62(25 Suppl):D42-50.
13. Moreira EM, Gall H, Leening MJ, Lahousse L, Loth DW, Krijthe BP, et al. Prevalence of Pulmonary Hypertension in the General Population: The Rotterdam Study. PLoS One. 2015;10(6):e0130072.

14. Lan NSH, Massam BD, Kulkarni SS, Lang CC. Pulmonary Arterial Hypertension: Pathophysiology and Treatment. Diseases. 2018;6(2).

15. Naeije R. Physiology of the pulmonary circulation and the right heart. Curr Hypertens Rep. 2013;15(6):623-31.

16. Kovacs G, Berghold A, Scheidl S, Olschewski H. Pulmonary arterial pressure during rest and exercise in healthy subjects: a systematic review. Eur Respir J. 2009;34(4):888-94.

17. Humbert M, Morrell NW, Archer SL, Stenmark KR, MacLean MR, Lang IM, et al. Cellular and molecular pathobiology of pulmonary arterial hypertension. J Am Coll Cardiol. 2004;43(12 Suppl S):13s-24s.

18. Apostolakis S, Konstantinides S. The right ventricle in health and disease: insights into physiology, pathophysiology and diagnostic management. Cardiology. 2012;121(4):263-73.

19. Dell'Italia LJ. Anatomy and physiology of the right ventricle. Cardiol Clin. 2012;30(2):167-87.

20. Haddad F, Hunt SA, Rosenthal DN, Murphy DJ. Right ventricular function in cardiovascular disease, part I: Anatomy, physiology, aging, and functional assessment of the right ventricle. Circulation. 2008;117(11):1436-48.

21. MacNee W. Pathophysiology of cor pulmonale in chronic obstructive pulmonary disease. Part One. Am J Respir Crit Care Med. 1994;150(3):833-52.

22. Santamore WP, Dell'Italia LJ. Ventricular interdependence: significant left ventricular contributions to right ventricular systolic function. Prog Cardiovasc Dis. 1998;40(4):289-308.

23. Dexter L. Atrial septal defect. Br Heart J. 1956;18(2):209-25.

24. Gillebert TC, Sys SU, Brutsaert DL. Influence of loading patterns on peak length-tension relation and on relaxation in cardiac muscle. J Am Coll Cardiol. 1989;13(2):483-90.

25. Naeije R, Badagliacca R. The overloaded right heart and ventricular interdependence. Cardiovasc Res. 2017;113(12):1474-85.

26. Hoeper MM, Humbert M, Souza R, Idrees M, Kawut SM, Sliwa-Hahnle K, et al. A global view of pulmonary hypertension. Lancet Respir Med. 2016;4(4):306-22.

27. Mandras SA, Mehta HS, Vaidya A. Pulmonary Hypertension: A Brief Guide for Clinicians. Mayo Clin Proc. 2020;95(9):1978-88.

28. Humbert M, Montani D, Evgenov OV, Simonneau G. Definition and classification of pulmonary hypertension. Handb Exp Pharmacol. 2013;218:3-29.

29. Galiè N, Hoeper MM, Humbert M, Torbicki A, Vachiery JL, Barbera JA, et al. Guidelines for the diagnosis and treatment of pulmonary hypertension. Eur Respir J. 2009;34(6):1219-63.

30. Awdish R, Cajigas H. Definition, epidemiology and registries of pulmonary hypertension. Heart Fail Rev. 2016;21(3):223-8.

31. Badesch DB, Champion HC, Sanchez MA, Hoeper MM, Loyd JE, Manes A, et al. Diagnosis and assessment of pulmonary arterial hypertension. J Am Coll Cardiol. 2009;54(1 Suppl):S55-66.

32. Douschan P, Kovacs G, Avian A, Foris V, Gruber F, Olschewski A, et al. Mild Elevation of Pulmonary Arterial Pressure as a Predictor of Mortality. Am J Respir Crit Care Med. 2018;197(4):509-16.

33. Badesch DB, Raskob GE, Elliott CG, Krichman AM, Farber HW, Frost AE, et al. Pulmonary arterial hypertension: baseline characteristics from the REVEAL Registry. Chest. 2010;137(2):376-87.

34. Mocumbi AO, Thienemann F, Sliwa K. A global perspective on the epidemiology of pulmonary hypertension. Can J Cardiol. 2015;31(4):375-81.

35. Sutton LL, Castro O, Cross DJ, Spencer JE, Lewis JF. Pulmonary hypertension in sickle cell disease. Am J Cardiol. 1994;74(6):626-8.

36. Knafl D, Gerges C, King CH, Humbert M, Bustinduy AL. Schistosomiasis-associated pulmonary arterial hypertension: a systematic review. Eur Respir Rev. 2020;29(155).

37. Bigna JJR, Sime PSD, Koulla-Shiro S. HIV related pulmonary arterial hypertension: epidemiology in Africa, physiopathology, and role of antiretroviral treatment. AIDS Research and Therapy. 2015;12(1):36.

38. Frost AE, Badesch DB, Barst RJ, Benza RL, Elliott CG, Farber HW, et al. The changing picture of patients with pulmonary arterial hypertension in the United States: how REVEAL differs from historic and non-US Contemporary Registries. Chest. 2011;139(1):128-37.

39. Ryan JJ, Archer SL. The right ventricle in pulmonary arterial hypertension: disorders of metabolism, angiogenesis and adrenergic signaling in right ventricular failure. Circ Res. 2014;115(1):176-88.

40. Haddad F, Doyle R, Murphy DJ, Hunt SA. Right ventricular function in cardiovascular disease, part II: pathophysiology, clinical importance, and management of right ventricular failure. Circulation. 2008;117(13):1717-31.

41. Naeije R, Manes A. The right ventricle in pulmonary arterial hypertension. Eur Respir Rev. 2014;23(134):476-87.

42. Ueno M, Miyauchi T, Sakai S, Kobayashi T, Goto K, Yamaguchi I. Effects of physiological or pathological pressure load in vivo on myocardial expression of ET-1 and receptors. Am J Physiol. 1999;277(5):R1321-30.

43. Rudski LG, Lai WW, Afilalo J, Hua L, Handschumacher MD, Chandrasekaran K, et al. Guidelines for the echocardiographic assessment of the right heart in adults: a report from the American Society of Echocardiography endorsed by the European Association of Echocardiography, a registered branch of the European Society of Cardiology, and the Canadian Society of Echocardiography. J Am Soc Echocardiogr. 2010;23(7):685-713; quiz 86-8.

44. Frost A, Badesch D, Gibbs JSR, Gopalan D, Khanna D, Manes A, et al. Diagnosis of pulmonary hypertension. Eur Respir J. 2019;53(1).

45. Galiè N, Humbert M, Vachiery JL, Gibbs S, Lang I, Torbicki A, et al. 2015 ESC/ERS Guidelines for the diagnosis and treatment of pulmonary hypertension: The Joint Task Force for the Diagnosis and Treatment of Pulmonary Hypertension of the European Society of Cardiology (ESC) and the European Respiratory Society (ERS): Endorsed by: Association for European Paediatric and Congenital Cardiology (AEPC), International Society for Heart and Lung Transplantation (ISHLT). Eur Heart J. 2016;37(1):67-119.

46. Hassani S. Principles of ultrasonography. J Natl Med Assoc. 1974;66(3):205-7, 31.

47. D'Alto M, Romeo E, Argiento P, Di Salvo G, Badagliacca R, Cirillo AP, et al. Pulmonary arterial hypertension: the key role of echocardiography. Echocardiography. 2015;32 Suppl 1:S23-37.

48. Augustine DX, Coates-Bradshaw LD, Willis J, Harkness A, Ring L, Grapsa J, et al. Echocardiographic assessment of pulmonary hypertension: a guideline protocol from the British Society of Echocardiography. Echo Res Pract. 2018;5(3):G11-g24.

49. Arkles JS, Opotowsky AR, Ojeda J, Rogers F, Liu T, Prassana V, et al. Shape of the right ventricular Doppler envelope predicts hemodynamics and right heart function in pulmonary hypertension. Am J Respir Crit Care Med. 2011;183(2):268-76.

50. Dabestani A, Mahan G, Gardin JM, Takenaka K, Burn C, Allfie A, et al. Evaluation of pulmonary artery pressure and resistance by pulsed Doppler echocardiography. Am J Cardiol. 1987;59(6):662-8.

51. Sohrabi B, Kazemi B, Mehryar A, Teimouri-Dereshki A, Toufan M, Aslanabadi N. Correlation between Pulmonary Artery Pressure Measured by Echocardiography and Right Heart Catheterization in Patients with Rheumatic Mitral Valve Stenosis (A Prospective Study). Echocardiography. 2016;33(1):7-13.

52. McLaughlin VV, Archer SL, Badesch DB, Barst RJ, Farber HW, Lindner JR, et al. ACCF/AHA 2009 expert consensus document on pulmonary hypertension a report of the American College of Cardiology Foundation Task Force on Expert Consensus Documents and the American Heart Association developed in collaboration with the American College of Chest Physicians; American Thoracic Society, Inc.; and the Pulmonary Hypertension Association. J Am Coll Cardiol. 2009;53(17):1573-619.

53. Dandel M, Lehmkuhl H, Knosalla C, Suramelashvili N, Hetzer R. Strain and strain rate imaging by echocardiography - basic concepts and clinical applicability. Curr Cardiol Rev. 2009;5(2):133-48.

54. Voigt JU, Cvijic M. 2- and 3-Dimensional Myocardial Strain in Cardiac Health and Disease. JACC Cardiovasc Imaging. 2019;12(9):1849-63.

55. Mondillo S, Galderisi M, Mele D, Cameli M, Lomoriello VS, Zacà V, et al. Speckle-tracking echocardiography: a new technique for assessing myocardial function. J Ultrasound Med. 2011;30(1):71-83.

56. Geyer H, Caracciolo G, Abe H, Wilansky S, Carerj S, Gentile F, et al. Assessment of myocardial mechanics using speckle tracking echocardiography: fundamentals and clinical applications. J Am Soc Echocardiogr. 2010;23(4):351-69; quiz 453-5.

57. Edvardsen T, Gerber BL, Garot J, Bluemke DA, Lima JA, Smiseth OA. Quantitative assessment of intrinsic regional myocardial deformation by Doppler strain rate echocardiography in humans: validation against three-dimensional tagged magnetic resonance imaging. Circulation. 2002;106(1):50-6.

58. Kalam K, Otahal P, Marwick TH. Prognostic implications of global LV dysfunction: a systematic review and meta-analysis of global longitudinal strain and ejection fraction. Heart. 2014;100(21):1673-80.

59. Muntean I, Benedek T, Melinte M, Suteu C, Togãnel R. Deformation pattern and predictive value of right ventricular longitudinal strain in children with pulmonary arterial hypertension. Cardiovasc Ultrasound. 2016;14(1):27.

60. Vitarelli A, Mangieri E, Terzano C, Gaudio C, Salsano F, Rosato E, et al. Three-dimensional echocardiography and 2D-3D speckle-tracking imaging in chronic pulmonary hypertension: diagnostic accuracy in detecting hemodynamic signs of right ventricular (RV) failure. J Am Heart Assoc. 2015;4(3):e001584.

61. Burkett DA, Slorach C, Patel SS, Redington AN, Ivy DD, Mertens L, et al. Left Ventricular Myocardial Function in Children With Pulmonary Hypertension: Relation to Right Ventricular Performance and Hemodynamics. Circ Cardiovasc Imaging. 2015;8(8).

62. Kallianos K, Brooks GC, Mukai K, Seguro de Carvalho F, Liu J, Naeger DM, et al. Cardiac Magnetic Resonance Evaluation of Left Ventricular Myocardial Strain in Pulmonary Hypertension. Acad Radiol. 2018;25(1):129-35.

63. Pedrizzetti G, Claus P, Kilner PJ, Nagel E. Principles of cardiovascular magnetic resonance feature tracking and echocardiographic speckle tracking for informed clinical use. J Cardiovasc Magn Reson. 2016;18(1):51.

64. Ryan J, Bloch K, Archer SL. Rodent models of pulmonary hypertension: harmonisation with the world health organisation's categorisation of human PH. Int J Clin Pract Suppl. 2011(172):15-34.

65. Vandamme TF. Use of rodents as models of human diseases. J Pharm Bioallied Sci. 2014;6(1):2-9.

66. Dumitrascu R, Koebrich S, Dony E, Weissmann N, Savai R, Pullamsetti SS, et al. Characterization of a murine model of monocrotaline pyrrole-induced acute lung injury. BMC Pulm Med. 2008;8:25.

67. Hill NS, Gillespie MN, McMurtry IF. Fifty Years of Monocrotaline-Induced Pulmonary Hypertension: What Has It Meant to the Field? Chest. 2017;152(6):1106-8.

68. Brittain E, Penner NL, West J, Hemnes A. Echocardiographic assessment of the right heart in mice. J Vis Exp. 2013(81).

69. Cheng HW, Fisch S, Cheng S, Bauer M, Ngoy S, Qiu Y, et al. Assessment of right ventricular structure and function in mouse model of pulmonary artery constriction by transthoracic echocardiography. J Vis Exp. 2014(84):e51041.

70. Wang Y, Tian W, Xiu C, Yan M, Wang S, Mei Y. Urantide improves the structure and function of right ventricle as determined by echocardiography in monocrotaline-induced pulmonary hypertension rat model. Clinical Rheumatology. 2019;38(1):29-35.

71. Badagliacca R, Papa S, Valli G, Pezzuto B, Poscia R, Reali M, et al. Right ventricular dyssynchrony and exercise capacity in idiopathic pulmonary arterial hypertension. Eur Respir J. 2017;49(6).

72. Diaba-Nuhoho P. Potential cardioprotective effect of chronic, moderate consumption of reduced-alcohol wine in a rat model of pulmonary hypertension: University of Cape Town; 2018.